nature cell biology

Local lung hypoxia determines epithelial fate decisions during alveolar regeneration

Ying Xi[1,6], Thomas Kim[1], Alexis N. Brumwell[1], Ian H. Driver[2], Ying Wei[1], Victor Tan[1], Julia R. Jackson[1], Jianming Xu[3], Dong-Kee Lee[3], Jeffrey E. Gotts[1], Michael A. Matthay[1], John M. Shannon[4], Harold A. Chapman[1,7,8] and Andrew E. Vaughan[1,5,6,7]

After influenza infection, lineage-negative epithelial progenitors (LNEPs) exhibit a binary response to reconstitute epithelial barriers: activating a Notch-dependent ΔNp63/cytokeratin 5 (Krt5) remodelling program or differentiating into alveolar type II cells (AEC2s). Here we show that local lung hypoxia, through hypoxia-inducible factor (HIF1α), drives Notch signalling and Krt5^{pos} basal-like cell expansion. Single-cell transcriptional profiling of human AEC2s from fibrotic lungs revealed a hypoxic subpopulation with activated Notch, suppressed surfactant protein C (SPC), and transdifferentiation toward a Krt5^{pos} basal-like state. Activated murine Krt5^{pos} LNEPs and diseased human AEC2s upregulate strikingly similar core pathways underlying migration and squamous metaplasia. While robust, HIF1α-driven metaplasia is ultimately inferior to AEC2 reconstitution in restoring normal lung function. HIF1α deletion or enhanced Wnt/β-catenin activity in Sox2^{pos} LNEPs blocks Notch and Krt5 activation, instead promoting rapid AEC2 differentiation and migration and improving the quality of alveolar repair.

The adult lung is a largely quiescent tissue but responds effectively to injury by activating stem/progenitor populations and promoting proliferation of surviving, mature lineages. Depending on the type and severity of cellular injury, different cell types are involved in repair[1–5]. A remarkable expansion of potentially regenerative ΔNp63^{pos}/Krt5^{pos} cells was observed in mouse lungs infected by murine-adapted H1N1 (PR8) influenza A virus[6]. Lineage-tracing experiments showed that >80% of the expanded Krt5^{pos} cells arise from LNEP populations in distal airways and probably alveoli[2]. These LNEPs proliferate and migrate dramatically to damaged sites to reconstitute the alveolar epithelium and promote recovery. Specific ablation of the newly expanded Krt5^{pos} cells by diphtheria toxin resulted in prolonged hypoxemia, confirming involvement of these cells in the repair process[7]. Notch signalling is critical for activating this ΔNp63/Krt5 remodelling program; however, persistent Notch signalling prevents alveolar epithelial differentiation[8], leading to cystic structures indicative of incomplete regeneration. Similar Krt5^{pos} honeycombing cysts also exist in the lungs from patients with pulmonary fibrosis, suggesting that common mechanisms apply to injury responses in both mice and humans[2].

In this study we explored the basis for activation and expansion of lung epithelial stem/progenitor cells observed in mice infected with H1N1 (PR8) influenza. Mice and humans infected with H1N1 influenza develop large areas virtually devoid of alveolar epithelial cells, requiring both expansion and migration of surviving AEC2s and more undifferentiated progenitors to restore alveolar epithelial barriers[2,9,10]. Studies here interrogate the underlying mechanisms and sources of epithelial progenitors that determine the alternative pathways of alveolar repair.

RESULTS

Influenza-activated Krt5^{pos} cells are derived from p63^{pos} lineage-negative progenitors

Our previous studies indicated that LNEPs are a Sox2^{pos} heterogeneous population comprised of both cells expressing the stem cell transcription factor ΔNp63 and ΔNp63^{neg} cells, although p63 expression was restricted to a minor LNEP fraction[2,11]. Transplantation studies suggested the possibility that these subtypes are biased toward either basal-like or AEC2 differentiation, respectively[2]. To clarify this, we infected tamoxifen-treated

[1]Department of Medicine, Cardiovascular Research Institute, UCSF, San Francisco, California 94143, USA. [2]Department of Anatomy, UCSF, San Francisco, California 94143, USA. [3]Department of Molecular and Cellular Biology, Baylor College of Medicine, Houston, Texas 77030, USA. [4]Division of Pulmonary Biology, Cincinnati Children's Hospital Medical Center, Cincinnati, Ohio 45229, USA. [5]Institute for Regenerative Medicine, University of Pennsylvania, Philadelphia, Pennsylvania 19104, USA. [6]Present addresses: Department of Immunology, Genentech Inc., South San Francisco, California 94080, USA (Y.X.); Department of Biomedical Sciences, School of Veterinary Medicine, University of Pennsylvania, Philadelphia, Pennsylvania 19104, USA (A.E.V.). [7]These authors jointly supervised this work.
[8]Correspondence should be addressed to H.C. (e-mail: hal.chapman@ucsf.edu)

Received 17 March 2017; accepted 21 June 2017; published online 24 July 2017; DOI: 10.1038/ncb3580

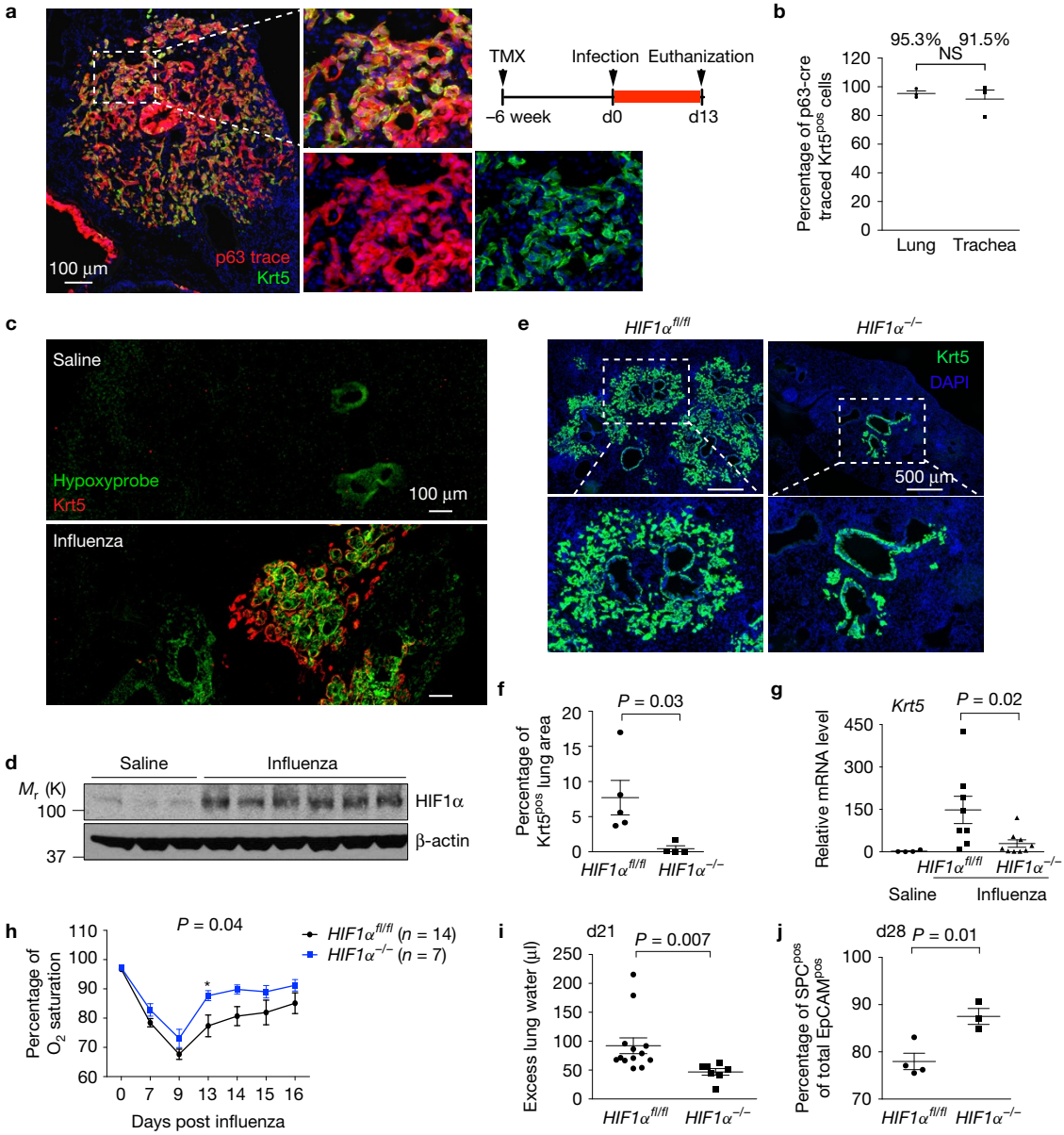

Figure 1 Epithelial HIF1α deletion blocks alveolar Krt5 activation post H1N1 infection. (**a**) Krt5^{pos} cells are completely traced (tdTomato^{pos}) after influenza injury in p63-CreERT2/tdTomato mice. (**b**) Quantification of lineage tracing by manual cell counts in tissue sections. Data are mean ± s.e.m., $n=3$ mice. (**c**) Krt5^{pos} cells (red) invariably appear in hypoxic alveolar regions (hypoxyprobe, green) after influenza injury in mice, although some Krt5^{neg} hypoxic regions were also observed ($n=7$ mice). (**d**) HIF1α protein accumulates in influenza-infected mouse lungs ($n=6$ influenza, $n=3$ saline, β-actin as loading control). (**e**) Alveolar Krt5^{pos} expansion (green) (left) is largely blocked by epithelial HIF1α deletion (right). (**f**) Quantification of **e**. Data are mean ± s.e.m., $n=5$ wild-type, $n=4$ *HIF1α*$^{-/-}$ mice from two independent experiments. (**g**) *Krt5* mRNA levels are reduced in *HIF1α*$^{-/-}$ mice. Data are mean ± s.e.m., $n=8$ wild-type, $n=9$ *HIF1α*$^{-/-}$ mice from 3 independent experiments. (**h**) Arterial oxygen saturation values obtained by pulse oximetry are greater in *HIF1α*$^{-/-}$ at the indicated times. (**i**) *HIF1α*$^{-/-}$ mice exhibit less excess lung water after influenza, indicative of improved barrier function. Data for **h** and **i** are mean ± s.e.m., $n=7$ *HIF1α*$^{-/-}$, $n=14$ wild-type (2 Shh-Cre^{neg}, 12 C57BL6) or $n=13$ wild-type for **i** (2 Shh-Cre^{neg}, 11 C57BL6) from two independent experiments. (**j**) AEC2 recovery/regeneration is improved in *HIF1α*$^{-/-}$ as judged by intracellular FACS for SPC^{pos} cells as a fraction of total EpCAM^{pos} cells. The percentage of EpCAM^{pos} live cells is unchanged in *HIF1α*$^{-/-}$ and wild-type mice. Data are mean ± s.e.m., $n=3$ *HIF1α*$^{-/-}$, $n=4$ wild-type mice from 2 independent experiments. Analysis is 11 days post-infection unless otherwise indicated. All *P* values were derived by unpaired two-tailed Student's *t*-test, except in **h**, derived by Mann–Whitney. NS, not significant. Unprocessed original scans of blots are shown in Supplementary Fig. 8.

p63-CreERT2 mice and determined that essentially all arising Krt5^{pos} cells were lineage labelled (Fig. 1a,b and Supplementary Fig. 1a). Uninjured mice possessed p63-lineage-labelled cells scattered throughout airways, comprising <0.01% of all lung epithelial cells (Supplementary Fig. 1b,c). These rare cells must possess remarkable resistance to infection as well as migratory and proliferative capacity. However, the scarcity of p63^{pos} LNEPs and their infrequent contribution to AEC2 regeneration (Supplementary Fig. 1a) suggest that additional p63^{neg} Sox2^{pos} LNEPs are a likely source of previously observed AEC2 differentiation following LNEP transplantation post

influenza injury[2]. To begin to dissect these possibilities we considered signals that impact LNEP expansion *in vivo*.

Epithelial HIF1α is required for Krt5^{pos} cell expansion post influenza injury

To explore mechanisms for p63^{pos} LNEP expansion during influenza infection, we examined the role of hypoxia, a likely consequence of extensive epithelial necrosis. Krt5^{pos} areas were found exclusively in hypoxic regions identified by immunostaining of pimonidazole (hypoxyprobe) (Fig. 1c). HIF1α, a key mediator of cell responses to hypoxia, accumulated in the whole lung lysates 11 days post infection (Fig. 1d), confirming that regions of the lung are hypoxic.

We then explored the functional relationship between hypoxia and Krt5^{pos} cell expansion/activation. Pan epithelial deletion of HIF1α (Shh-Cre; *HIF1α*$^{fl/fl}$, designated as *HIF1α*$^{-/-}$) results in viable mice, born at expected Mendelian ratios, and displaying no overt defects, while epithelial *HIF1α* messenger RNA was decreased by 99% (Supplementary Fig. 1d–f). Eleven days after influenza injury, the *HIF1α*$^{-/-}$ mice showed a dramatic decrease in alveolar Krt5^{pos} cell expansion (Fig. 1e–f), as well as Krt5 protein (Supplementary Fig. 2a) and mRNA (Fig. 1g) levels, with no inhibition of airway Krt5^{pos} expansion. Expansion of LNEPs was attenuated, demonstrated by a lack of integrin β4^{pos} and p63^{pos} expanding cells (Supplementary Fig. 2b,c). We next addressed the possibility that *HIF1α*$^{-/-}$ mice were less injured. Regardless of HIF1α deletion, viral protein was detected on day 4 and cleared by day 11 (Supplementary Fig. 2d). Both groups lost 20–30% weight (Supplementary Fig. 2e) and no difference was observed in the inflammatory cell counts or protein levels in bronchoalveolar lavage (Supplementary Fig. 2f,g). Comparable large regions depleted of alveolar epithelial cells developed in all mice (Supplementary Fig. 2h,i). *HIF1α*$^{-/-}$ mice are therefore injured at similar levels as wild-type mice, but lack alveolar Krt5^{pos} cell expansion.

HIF1α deletion promotes functional regeneration

While injury levels were equivalent, epithelial *HIF1α*$^{-/-}$ mice regained weight more rapidly after the acute injury phase (Supplementary Fig. 2j). Remarkably, arterial oxygen saturation in *HIF1α*$^{-/-}$ mice also recovered more quickly, and barrier function was likewise improved as judged by less interstitial and/or alveolar edema (Fig. 1h,i and Supplementary Fig. 2k). Furthermore, AEC2s constituted a higher fraction of the total epithelium in *HIF1α*$^{-/-}$ mice after recovery (Fig. 1j). To address the source of the newly generated AEC2s, we deleted HIF1α specifically in Sox2^{pos} cells, including both p63^{pos} and p63^{neg} LNEPs but not AEC2s, with Sox2-CreERT2/tdTomato mice (Fig. 2a). HIF1α deletion from the Sox2^{pos} lineage resulted in strong attenuation of alveolar Krt5^{pos} cell expansion after infection (Fig. 2b), similar to global epithelial HIF1α deletion (Fig. 1e). Instead, the majority of Sox2-traced alveolar cells exhibited AEC2 differentiation, as judged by location and SPC expression (Fig. 2a,c). Sox2-labelled AEC2s were much more proliferative than either endogenous AEC2s in the same injured regions or AEC2s in influenza-injured lungs of mice with HIF1α deletion specifically in pre-existing AEC2s (Fig. 2d,e). While HIF1α-driven Krt5^{pos} expansion supports some degree of functional recovery[7], HIF1α deletion substantially improves lung function by re-directing airway progenitor responses toward rapid AEC2 expansion and migration, bypassing basal-like metaplasia entirely. Given the impact of HIF1α on the quality of epithelial recovery, we explored the mechanistic link between hypoxia and Krt5^{pos} cell expansion.

Hypoxia promotes Notch signalling and Krt5 expression in a HIF1α-dependent manner

We validated that submersion cultures are hypoxic, as previously reported[12], in comparison with air/liquid interface demonstrated by hypoxyprobe staining and elevation of HIF1α targets (Fig. 3a). Hypoxia also promoted Notch target and *Krt5* mRNA expression (Fig. 3a), suggesting that HIF1α regulates Notch activity. Primary LNEP-enriched cells (EpCAM^{pos} integrin β4^{pos}) expressed negligible *Krt5* but its expression dramatically increased during the first 7–10 days *in vitro*, and continued over several passages alongside other basal cell genes (Fig. 3b). In contrast, LNEPs isolated from *HIF1α*$^{-/-}$ mice expressed lower levels of basal cytokeratins and Notch target genes, indicating that HIF1α is required for Notch activity. *HIF1α*$^{-/-}$ LNEPs formed fewer and smaller colonies (Fig. 3e and Supplementary Fig. 3a,b) but demonstrate increased SPC expression (Fig. 3c,d and Supplementary Fig. 3c) consistent with the suppressive effects of Notch signalling on alveolar differentiation[2,8,13,14].

Because HIF1α loss had no effect on total NICD1 level (Fig. 3f), we tested whether HIF1α could promote NICD DNA binding via chromatin immunoprecipitation (ChIP) experiments. Both HIF1α and NICD1 associated with CSL-binding sites (CBE) and HIF1α-binding sites (HRE) on *Krt5, Hey1* and *Hes5* promoters (Fig. 3g and Supplementary Fig. 3d). NICD1 binding on DNA was abolished by HIF1α deletion. Multiple binding sites on the promoters were tested and all showed similar results.

To confirm Notch signalling as a driver of LNEP expansion, we analysed the transcriptomes of highly purified quiescent LNEPs (EpCAM^{pos} β4^{pos} CC10^{neg} FoxJ1^{neg}) (Supplementary Fig. 3e) and activated LNEPs (Krt5-CreERT2 traced cells 17 days post infection). Activated LNEPs showed high induction of Notch and HIF1α target genes and *Krt5* expression (Fig. 3h). The loss of Notch activity in HIF1α-deficient cells correlates directly with the failure of Krt5^{pos} cell expansion *in vivo* in *HIF1α*$^{-/-}$ mice. Thus, injury-induced hypoxia, through HIF1α, drives Notch activity by empowering NICD binding on Notch target gene promoters, and promoting LNEP differentiation towards Krt5^{pos} basal-like cells. Of note, HIF1α deletion had little apparent effect on Notch regulation of airway epithelium[15–17] (Supplementary Fig. 3f,g).

Stabilization of β-catenin promotes LNEP differentiation towards AEC2s

Because Wnt signalling is important for the development of alveolar epithelium[18–21], we tested whether activating Wnt could promote LNEP differentiation into AEC2s *in vivo*, similar to HIF1α deletion. We crossed Sox2-CreERT2/tdTomato mice with β-catenin gain-of-function mice (β-catenin^{loxEx3}) to stabilize β-catenin in Sox2^{pos} LNEPs. β-catenin stabilization in Sox2-traced cells (tdTomato^{pos}) led to ectopic SPC expression in the airways even without challenge, demonstrating that Wnt activity alone could induce a fate change even in quiescent adult progenitors (Supplementary Fig. 4a). Expression of SPC and expression of Scgb3a2 (a highly specific club cell marker)[22,23] were largely mutually exclusive, and previous reports activating

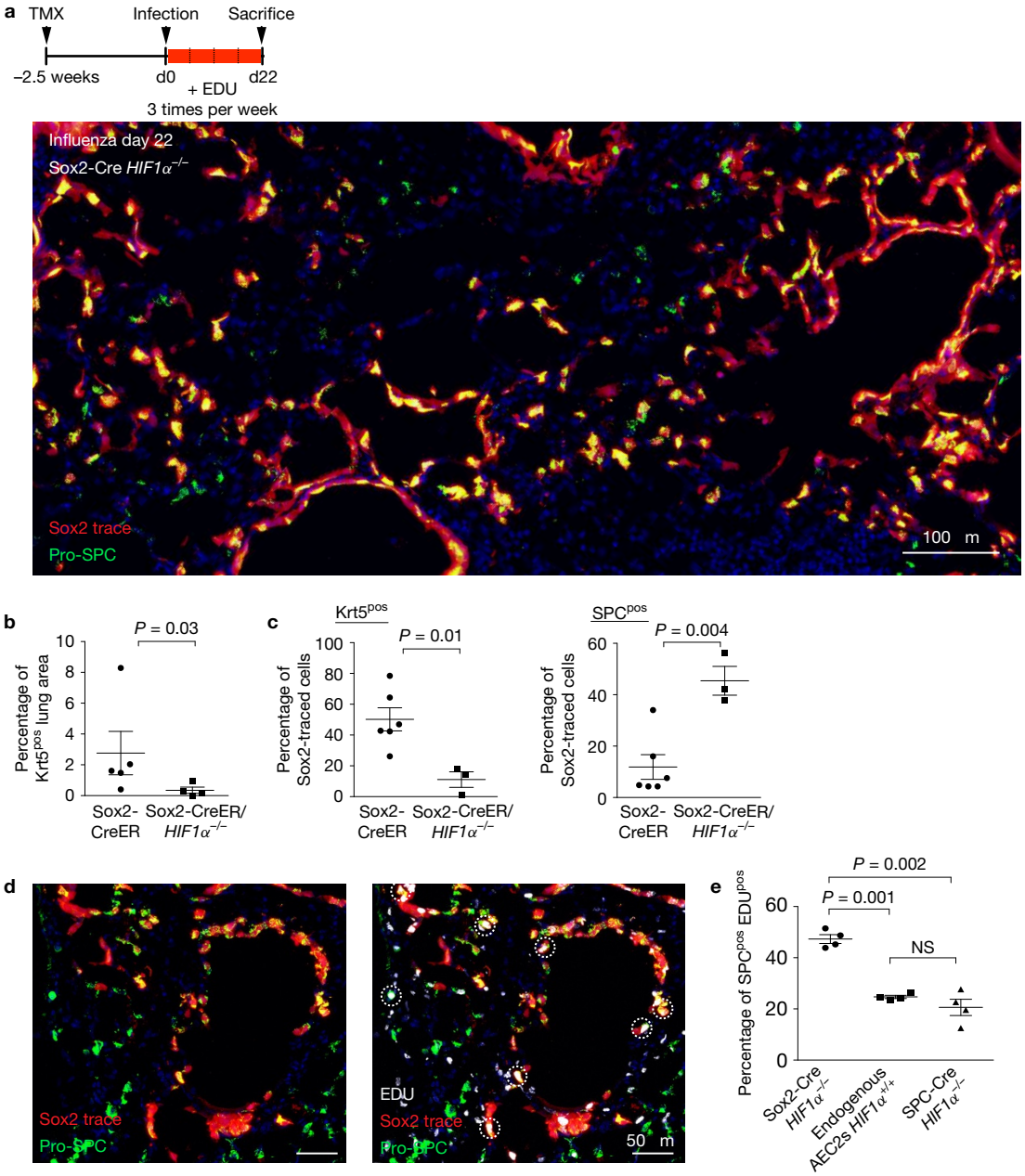

Figure 2 HIF1α deletion in Sox2^{pos} LNEPs promotes regeneration of AEC2s. (**a**) HIF1α deletion with Sox2-CreERT2 prior to infection results in abundant SPC^{pos} (green) traced cells by 22 days post-influenza. (**b**) HIF1α deletion in Sox2^{pos} cells blocks Krt5 expansion as in pan-epithelial deletion (Fig. 1f). (**c**) Sox2^{pos} cell fate is redirected from Krt5^{pos} to SPC^{pos} cells as determined by relative fractions of total alveolar Sox2-traced cells. (**d**) Newly generated Sox2-traced, *HIF1α*$^{-/-}$ AEC2s incorporate more EDU (white) than nearby, endogenous AEC2s or AEC2s with HIF1α deletion (utilizing SPC-CreERT2 mice). (**e**) Quantification of **d**, as the fraction of total traced or untraced SPC^{pos} cells that are also EDU^{pos}. Data are mean ± s.e.m.; $n=4$ Sox2-CreERT2/*HIF1α*$^{-/-}$ in **b**,**e**; $n=5$ Sox2-CreERT2/*HIF1α*$^{+/+}$ in **b**; $n=3$ Sox2-CreERT2/*HIF1α*$^{-/-}$, $n=6$ Sox2-CreERT2/*HIF1α*$^{+/+}$ in **c**; $n=4$ SPC-CreERT2/*HIF1α*$^{-/-}$ in **e**. Sox2-CreERT2/*HIF1α*$^{+/+}$ mice are denoted as 'Sox2-CreER' on the axis. Analysis is 22 days post-infection. *P* values derived by Mann Whitney in **b** and unpaired *t*-test with Welch's correction in **c**,**e**.

β-catenin in mature club cells resulted in no increase in SPC expression[24], indicating that most newly arising SPC^{pos} cells were derived from Sox2^{pos} LNEPs and not mature club cells. After infection, Sox2-traced cells expanded and differentiated primarily into Krt5^{pos} cells, whereas β-catenin stabilization dramatically switched differentiation from Krt5^{pos} to SPC^{pos}, leading to AEC2 expansion (Fig. 4a,b).

We further explored the impact of Notch and Wnt signalling on LNEP differentiation *in vitro*. Treatment with the GSK3β inhibitor CHIR99021 inhibited Notch and hypoxia target gene expression while activating Wnt target gene *Axin2* expression (Fig. 4c), indicating that Wnt activity antagonizes Notch and hypoxia signalling, favouring AEC2 differentiation of LNEPs (Fig. 4d). ChIP experiments indicated that the inhibition occurs by prevention of NICD1 and HIF1α association on target promoters, without affecting NICD1 protein level (Fig. 4e,f and Supplementary Fig. 4b). We established clonal cultures of fluorescently tagged LNEPs and observed multiple instances of Krt5^{pos}

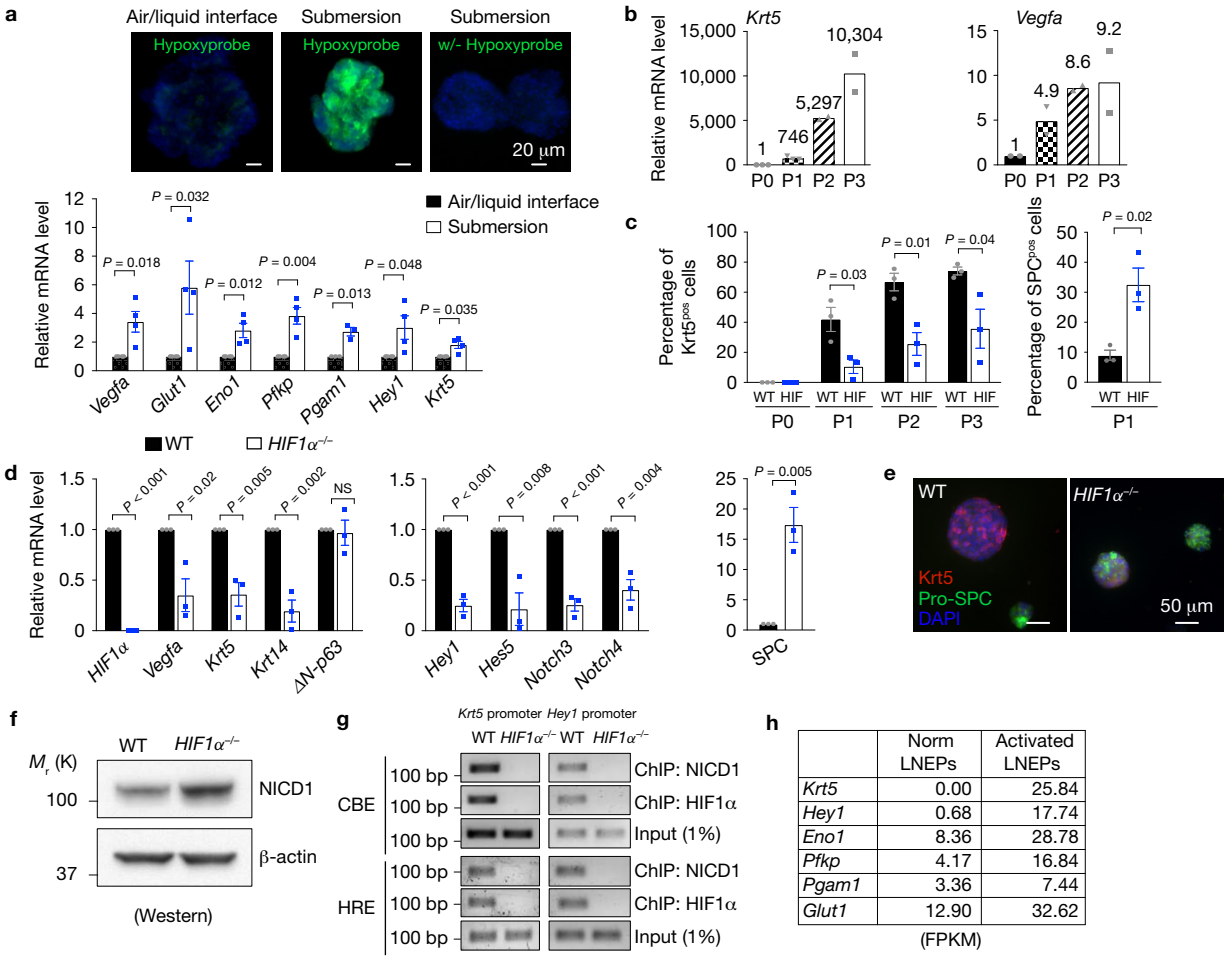

	Norm LNEPs	Activated LNEPs
Krt5	0.00	25.84
Hey1	0.68	17.74
Eno1	8.36	28.78
Pfkp	4.17	16.84
Pgam1	3.36	7.44
Glut1	12.90	32.62

(FPKM)

Figure 3 HIF1α drives Notch signalling *in vitro* and *in vivo*. (**a**) LNEPs in submersion culture are hypoxic (hypoxyprobe, green) in comparison with LNEPs in air/liquid interface culture. Submersion results in upregulation of hypoxia and Notch target genes as well as *Krt5*. Data are mean ± s.e.m., $n = 4$ independent experiments. (**b**) *Krt5* and *Vegfa* mRNA increase with time (passage) in cultured LNEPs. P0, primary cells, P1–P3, passages, $n = 2$ independent experiments. (**c**) HIF1α-deficient LNEPs exhibit reduced Krt5 and increased SPC expression as measured by the percentage of positive cells in culture. WT, wild-type; HIF, *HIF1α*$^{-/-}$. (**d**) Expression levels of basal cytokeratins and Notch target genes are similarly reduced in *HIF1α*$^{-/-}$ LNEPs, in contrast to elevated *SPC* expression. In **c**,**d**, data are mean ± s.e.m. from $n = 3$ independent experiments. (**e**) Representative images of P1 colonies (primary cells cultured for 1 week) showing smaller colony size, reduced Krt5 and increased SPC expression in HIF1α-deficient LNEPs culture. (**f**) Representative blots of three independent experiments showing that the NICD1 protein level is not affected by HIF1α deletion in cultured LNEPs. (**g**) HIF1α and NICD1 associate with both CSL-binding element (CBE) and HIF-responsive element (HRE) on the *Krt5* and *Hey1* promoters by ChIP. HIF1α deletion completely prevents NICD1 association on promoter DNA. See qPCR quantification as well as *Hes5* promoter analysis from three independent experiments in Supplementary Fig. 3d. (**h**) RNA-Seq results showing that activated LNEPs (Krt5-CreERT2 traced cells 17 days post infection) have higher *Krt5*, Notch and hypoxia target gene expression as compared with LNEPs from uninfected mice ($n = 5$ mice per group). *P* values derived by unpaired two-tailed Student's *t*-test, except in **a**, derived by one-sample *t*-test. Unprocessed original scans of blots are shown in Supplementary Fig. 8.

and SPC^{pos} cells in a single-colour clone, indicating that both cell types could arise from a single cell (Fig. 4g and Supplementary Fig. 4c), although some colonies were homogeneously Krt5^{pos} or SPC^{pos}. Likewise, p63^{neg} LNEPs isolated from tamoxifen-treated p63-CreERT2 mice demonstrated ~10% recombination after one culture passage following addition of 4OHT (Supplementary Fig. 4d), confirming differentiation of p63^{neg} to p63^{pos} cells. Most p63^{neg} LNEPs in culture expand as either undifferentiated cells or as SPC^{pos} cells, the latter significantly enhanced by Wnt activation (Fig. 4d and Supplementary Fig. 4d). Therefore, stabilization of β-catenin blocks Notch and hypoxia signalling, attenuates Krt5 activation, and promotes AEC2 expansion after influenza infection. Interestingly, while Krt5^{pos} cells *in vitro* arise from p63^{neg} LNEPs (Supplementary Fig. 4d), following influenza infection, activated Krt5^{pos} cells *in vivo* are derived virtually entirely from rare LNEPs already expressing p63 (Fig. 1a), suggesting that p63^{neg} LNEPs *in vivo* are intrinsically slower to differentiate to Krt5^{pos} cells or rendered dysfunctional by H1N1 infection.

Deleting HIF1α or stabilizing β-catenin does not alter LNEP differentiation after full Notch/Krt5 activation.

To investigate the possibility of LNEP transdifferentiation to AEC2s after Krt5 activation, we crossed Krt5-CreERT2; tdTomato mice with either *HIF1α*$^{fl/fl}$ or β-catenin^{loxEx3} mice and treated with tamoxifen 7–10 days post infection to delete HIF1α or stabilize β-catenin specifically in activated LNEPs. Neither blocking HIF1α nor activating Wnt signalling altered Krt5^{pos} cell fate: Krt5 traced cells did not give

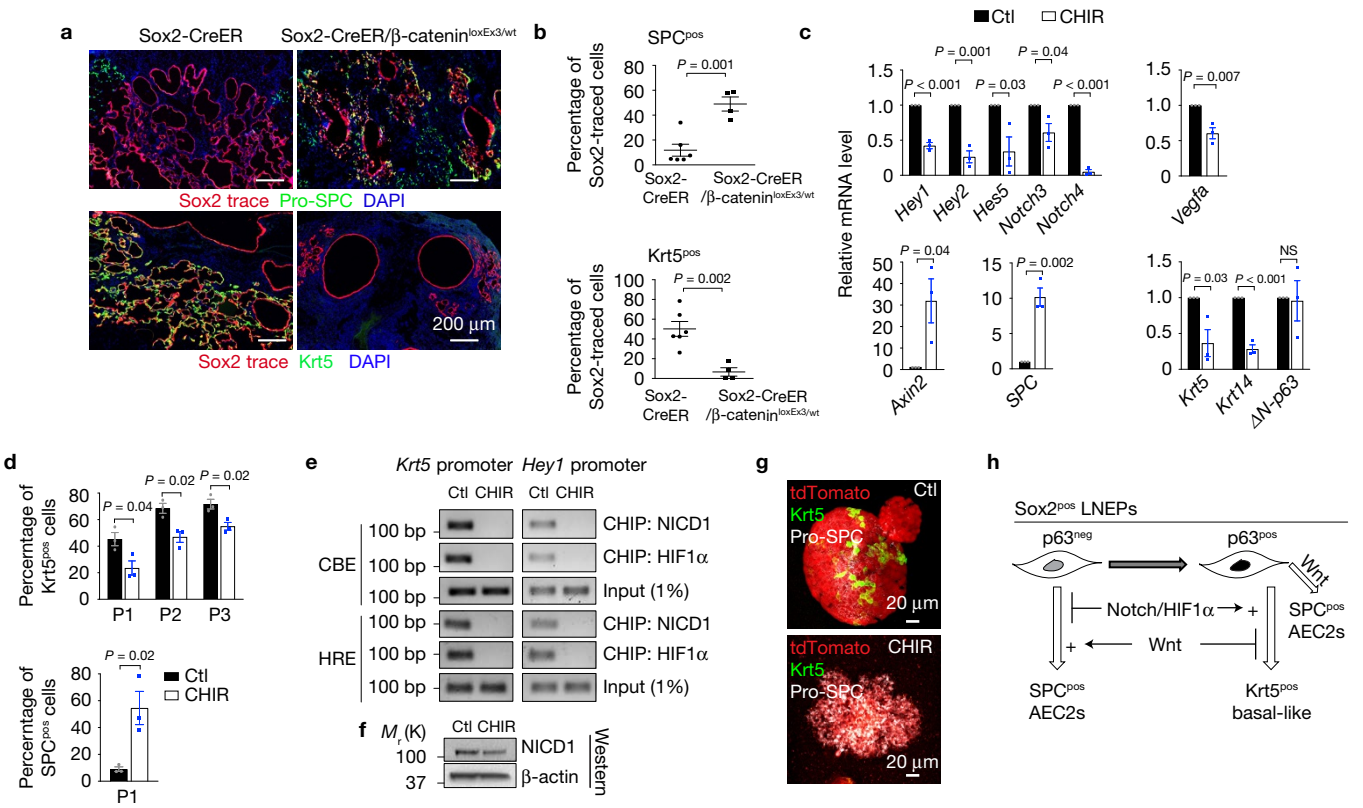

Figure 4 Stabilization of β-catenin promotes LNEP differentiation towards an alveolar fate. (**a**) Krt5^{pos} cells and to a lesser degree SPC^{pos} cells are traced by Sox2-CreERT2 in response to influenza injury (left). Stabilization of β-catenin in Sox2-expressing cells prior to injury by tamoxifen administration results in a dramatic increase in traced SPC^{pos} cells and concurrent decrease in Krt5^{pos} cells (right). (**b**) Quantification of the percentage of the Sox2-CreERT2 traced cells expressing Krt5 (bottom) or SPC (top) in injured alveolar areas. Data are mean ± s.e.m., $n=4$ with β-catenin stabilization, $n=6$ without (same mice from Fig. 2c) from two independent experiments. (**c**) CHIR99021 treatment phenocopies HIF1α deletion (see Fig. 3d), reducing expression of Notch and HIF1α target genes and basal cytokeratins while increasing *SPC* and *Axin2* by qPCR analysis. (**d**) Wnt agonism of LNEPs *in vitro* decreases the frequency (%) of Krt5^{pos} cells with a concurrent increase of SPC^{pos} cells in cytospin analysis. In **c**,**d**, data are mean ± s.e.m. from $n=3$ independent experiments. (**e**) CHIR99021 treatment further mirrors HIF1α deletion in preventing association of NICD1 and HIF1α with CBE and HRE sites on the *Krt5* and *Hey1* promoters as determined by ChIP. See qPCR quantification as well as *Hes5* promoter analysis from three independent experiments in Supplementary Fig. 4b. (**f**) Representative blots of three independent experiments showing that the NICD1 protein level is not affected by β-catenin stabilization. (**g**) LNEPs isolated from ubGFP (GFP^{pos}) and mTmG (tdTomato^{pos}) were mixed in equal ratios and cultured resulting in largely single-colour colonies (clones). Representative images of tdTomato^{pos} colonies demonstrate SPC^{pos} and Krt5^{pos} cells in single clones whereas most colonies exhibit uniform SPC expression when treated with GSK3β inhibitor CHIR99021 (2 nM). Krt5 is pseudocoloured green for visualization since these colonies were uniformly tdTomato^{pos}. (**h**) Schematic model of Sox2^{pos} LNEP activation in mouse lungs in response to severe injury. HIF1α/Notch promotes Krt5^{pos} basal-like cell expansion from p63^{pos} LNEPs. Wnt/β-catenin signalling antagonizes hypoxia and Notch signalling and promotes AEC2 expansion from p63^{neg} LNEPs. LNEPs that upregulate p63 can still respond to Wnt signals to generate AEC2s (see Supplementary Fig. 4d). *P* values were derived by unpaired two-tailed Student's *t*-test. Unprocessed original scans of blots are shown in Supplementary Fig. 8.

rise to AEC2s two weeks post tamoxifen, retaining Krt5 expression and Notch activity (Supplementary Fig. 5). In the context of severe influenza infection, it appears that once the Notch/Krt5 program is activated, signals that redirect initial LNEP differentiation become ineffective in inducing transdifferentiation of Krt5-committed cells.

Krt5^{pos} expansion represents a common response to major lung injury in both mice and humans

As hyperactive Notch/Krt5^{pos} cysts exist in lungs from patients with pulmonary fibrosis[2], we examined whether the expansion of Krt5^{pos} cells is a common response to major injury. In lung tissue obtained from six patients who succumbed to H1N1 influenza A virus there was widespread destruction of parenchymal cells and three patient samples evidenced an extensive regenerative response (Fig. 5a,b). Large areas were devoid of SPC^{pos} AEC2s and comprised instead of Krt5^{pos} cells that appear flattened and cover much of the alveolar surfaces, reminiscent of LNEP expansion in influenza-infected mouse lungs. In contrast to mice, some areas of affected lung contained numerous Krt5^{pos} cells that were also clearly positive for SPC, suggesting either differentiation of Krt5^{pos} cells toward AEC2s or transdifferentiation of AEC2s toward basal-like cells. This was paralleled in sections from ARDS (acute respiratory distress syndrome) lungs (Fig. 5c) and by prior observations in scleroderma in which SPC^{pos} /Krt5^{pos} alveolar cells were observed[2]. We conclude that as in murine influenza injury, human stem/progenitor cells demonstrate robust attempts at re-establishing alveolar epithelial barriers with Krt5^{pos} cells. Although variable, HIF1α protein was also increased in all idiopathic pulmonary fibrosis (IPF) samples relative to normal lungs, consistent with reports of hypoxia signalling in IPF[25,26] (Fig. 5d). To further investigate the relationship between hypoxia and Krt5^{pos} cell expansion in tissue

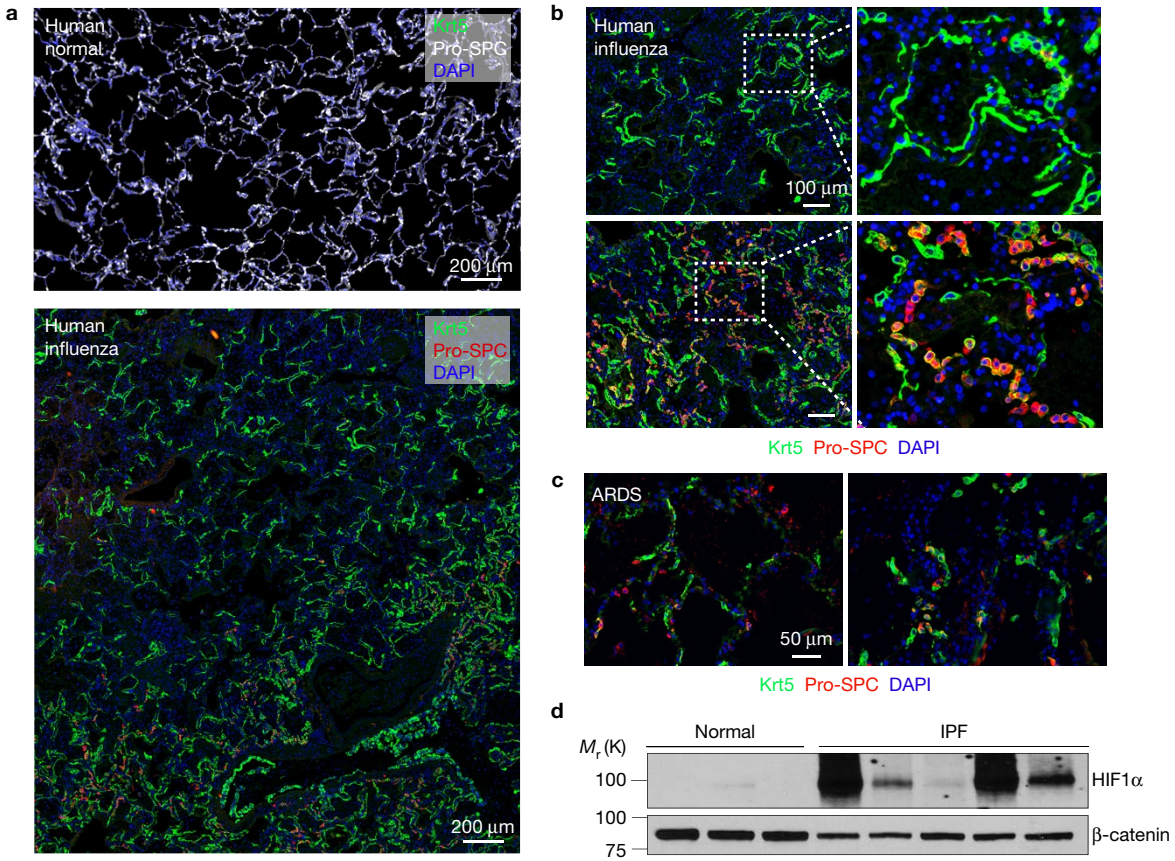

Figure 5 Krt5^{pos} cell expansion is a common response of human lung epithelium to major injury. (**a**,**b**) Representative images demonstrating Krt5^{pos} (green) epithelial expansion into the alveolar parenchyma in H1N1 influenza-injured human lungs. Regions of cells co-expressing Krt5 and pro-SPC (red) are also observed (**b**). (**c**) Krt5^{pos} expansion and Krt5/SPC double-positive cells are also present in ARDS lungs. (**d**) Representative blot of two independent experiments showing HIF1α accumulation in the lungs of IPF patients ($n=9$ IPF, $n=7$ normal in total, β-catenin as loading control), indicating that hypoxia occurs in IPF lungs. Unprocessed original scans of blots are shown in Supplementary Fig. 8.

repair, we employed single-cell transcriptional profiling of epithelial cells isolated from freshly explanted diseased human lungs.

Evidence that Notch and hypoxia regulate human lung epithelial repair processes

We performed single-cell RNA-Seq using the Fluidigm C1 to analyse the transcriptomes of AEC2s (HTII-280^{pos}, of which 98% express SPC)[27] and basal-enriched cells (integrin α6^{pos} HTII-280^{neg}, of which 50–70% express Krt5) (Supplementary Fig. 6). We sequenced between 25 and 72 single cells from normal lungs as well as lungs from patients diagnosed with scleroderma, dyskeratosis congenita and IPF, all fibrotic diseases despite differing etiologies. Principal component analysis (PCA) and whole-genome unsupervised hierarchical clustering clearly separated AEC2s from normal and fibrotic lungs (Supplementary Fig. 7a). The Notch targets *HES1*[28] and *SCGB3A2*[22] were among the most differentially expressed genes in diseased versus normal populations, corroborating our findings in fibrotic human lungs (Supplementary Table 1). Furthermore, HIF1α stands out as a top upstream regulator in the diseased AEC2s based on ingenuity pathway analysis (IPA, QIAGEN, www.qiagen.com/ingenuity) (Supplementary Table 2).

We generated a hypoxia-induced gene expression signature by combining three published hypoxia signatures[29,30] (IPA HIF1α pathway). Hierarchical clustering based on the hypoxia signature plus Notch target *HES1*, *KRT5* and AEC2 markers showed three distinct populations: normal AEC2s (Groups I and II), pathologic AEC2s with a hypoxia signature and high *HES1* (Group III), and pathologic AEC2s with hypoxia targets and *HES1*, but decreased surfactants and upregulated basal cytokeratins (Group IV) (Fig. 6a–c and Supplementary Table 3). Adding normal basal-enriched cells (Group V) demonstrated that Group IV was transcriptionally more similar to basal-enriched cells than normal AEC2s. Groups I and II contained nearly all cells isolated from normal lungs that do not clearly segregate based on unbiased clustering, suggesting that the mild hypoxia target expression in Group II may be a technical artefact (Fig. 6d and Supplementary Table 4). Adding 27 AEC2s from IPF lungs placed most IPF cells in Group IV (Supplementary Fig. 7b). Clustering based on the entire transcriptome except the hypoxia signature and lineage markers resulted in nearly identical clustering, validating the hypoxia signature in predictive categorization and demonstrating that meaningful whole-transcriptome (phenotypic) changes occur coordinately with hypoxia signalling (Supplementary Fig. 7c).

The expression pattern transitions from normal cells to basal-like cells in Group IV, which is surprisingly similar to normal basal-enriched cells (Group V) (Fig. 6e and Supplementary Table 5). Importantly, while Group IV cells develop a basal-like transcriptome

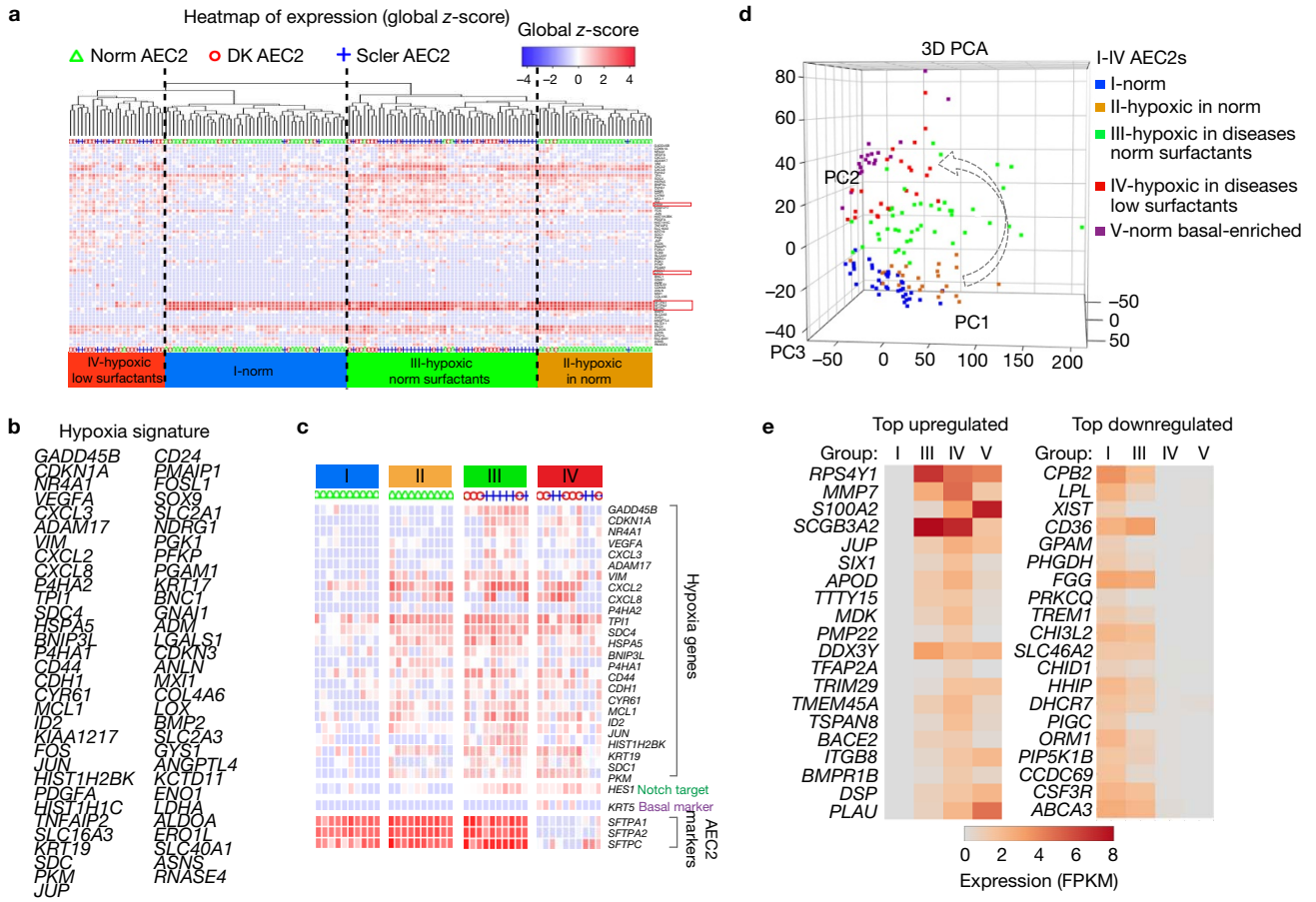

Figure 6 Single-cell RNA-Seq analysis of primary human lung epithelial cells from normal and fibrotic lungs indicates hypoxia/Notch signalling promotes AEC2s transdifferentiation towards basal-like cells after major injury. (**a**) Hierarchical clustering of single-cell transcriptomes of AEC2s (HTII-280^{pos}) (columns) isolated from normal (triangles), dyskeratosis congenita (DK) (circles), and scleroderma (crosses) lung explants. Clustering reflects hypoxia signature genes (listed in panel **b**) plus *STFPA1*, *STFPA2*, *SFTPC*, *KRT5* and *HES1* (highlighted with red boxes) (rows). Four distinct groups (I–IV) are highlighted in different colours: normal AEC2s (Group I, blue), normal AEC2s with hypoxic gene expression (Group II, yellow), AEC2s from diseases with hypoxia signature and *HES1* (Group III, green), and AEC2s from diseases with hypoxia signature and *HES1*, with concurrent loss of surfactants and acquisition of *Krt5* (Group IV, red). (**b**) List of hypoxia signature genes. (**c**) Representative cells and genes of the four groups. (**d**) Whole-genome PCA analysis of the four groups plus normal basal-enriched cells (HTII-280$^{neg}\alpha6^{pos}$, Group V) demonstrates progressive evolution to basal cell-like expression profiles in diseased AEC2s. (**e**) The expression pattern of the top 20 up- and downregulated genes derived from ANOVA analysis of Group IV versus I, showing the progressive transition from Group I to Group IV, which is very similar to Group V basal-enriched cells. The average FPKM values of the indicated genes averaged within each group (I–V) are displayed in the heatmap.

(Fig. 6d,e), most cells retain significant reads for *SFTPC* whereas no *SFTPC* was detected in any of the basal-enriched cells. Furthermore, culture of normal AEC2s resulted in marked upregulation of *KRT5* mRNA, which was attenuated by Notch inhibition (Supplementary Fig. 7d). These data support a scenario in which human epithelial progenitors utilize a common injury response pathway characterized by hypoxia/Notch/Krt5 and progressively transdifferentiate to a basal-like phenotype in diverse disease and injury settings.

A subset of human alveolar epithelial cells, distal airway cells, and murine LNEPs share a migratory gene expression profile

Activated murine LNEPs and Group IV hypoxic AEC2s shared 102 upregulated genes and 25 downregulated genes (Fig. 7a and Supplementary Fig. 7e and Supplementary Table 6). IPA analysis of the common upregulated genes indicates that HIF1α is a top upstream regulator (Supplementary Table 7) and cell movement/invasion and proliferation are the top two processes affected (Supplementary Tables 8,9). Importantly, normal human distal airway basal-enriched cells (Group V) appear inherently primed by expression of the motility-linked genes induced by hypoxia/Notch in AEC2s (Supplementary Fig. 7e).

We therefore compared motility of human basal-enriched cells with normal human AEC2s. Basal-enriched cells and activated LNEPs were highly motile *in vitro* in comparison with AEC2s (Fig. 7b). We further analysed the function of two of these motility genes, *AXL* and *EPHA2*[31,32], which encode receptor tyrosine kinases. Inhibition of AXL or EPHA2 markedly blocked LNEP migration (Fig. 7c). We conclude that hypoxia/Notch activates a proliferative/migratory program in multiple human cell types, implying a common strategy to replenish epithelial barriers under hypoxic, stressful conditions.

DISCUSSION

The lung is highly efficient at matching air and blood over its enormous alveolar surface area, ensuring oxygen uptake and

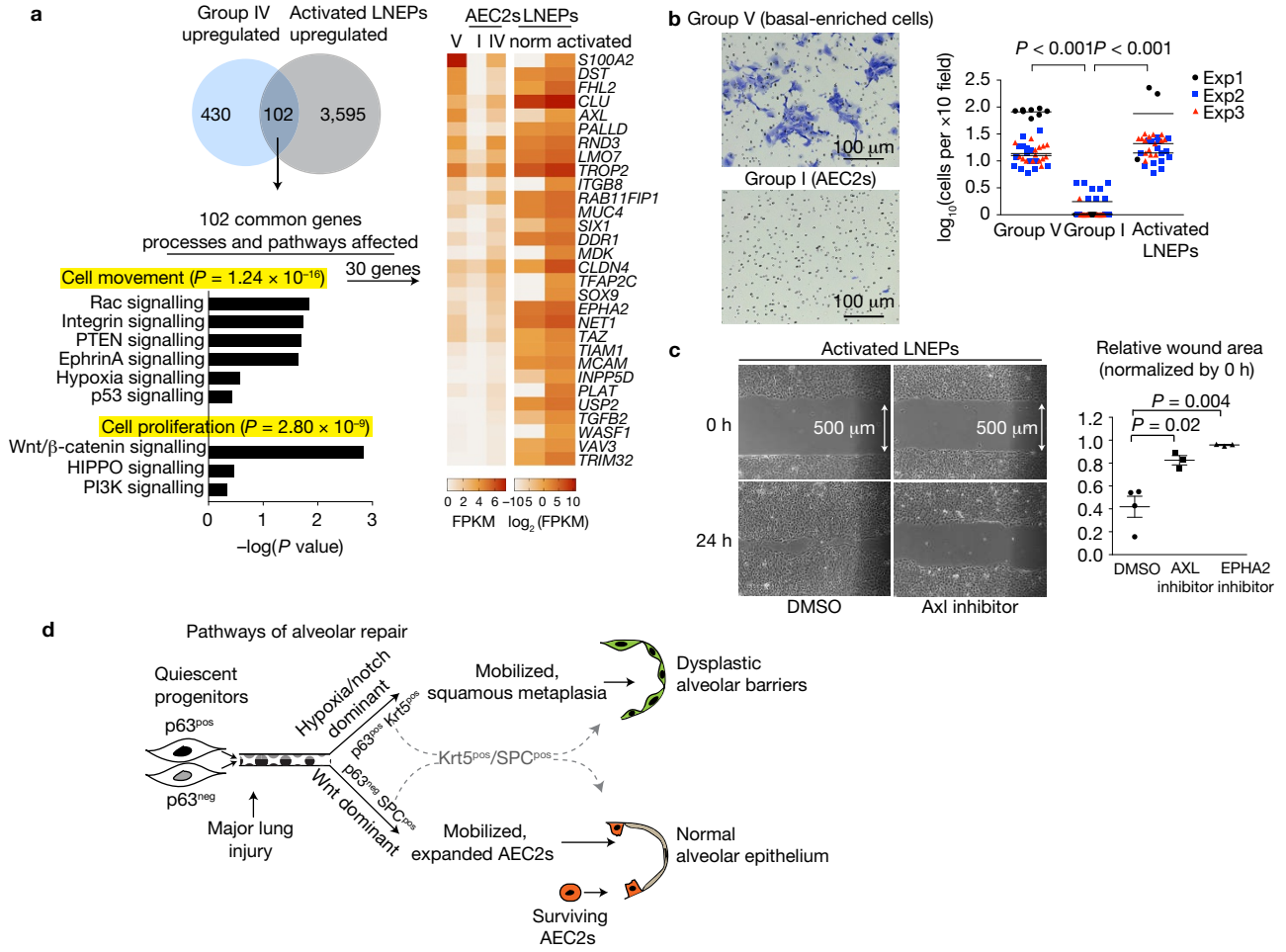

Figure 7 Both human and mouse lung epithelial progenitor cells activate hypoxia/Notch signalling and a motile phenotype in response to major injury. (**a**) Overlap between mouse activated LNEPs (Krt5^{pos} cells versus quiescent LNEPs) and human hypoxic AEC2s (Group IV versus I) identifies pathways strongly implicated in cell movement. Average FPKM values of human cells (Group I, IV and V), and mouse quiescent and activated LNEPs from RNA-Seq are indicated in the heatmap (right) for 30 of these 102 genes directly implicated in migration. IPA analysis of these 102 genes implicates cell movement and cell proliferation as major cellular processes affected, with at least 30 reported to promote cell migration. (**b**) Human Group V basal-enriched cells are strikingly motile in a transwell assay, similar to activated LNEPs. Cells that migrated through the pores to the bottom of the insert were stained and quantified. Data are mean ± s.e.m. from $n = 3$ independent experiments. (**c**) Two tyrosine kinases identified from the common 102 genes, *AXL* and *EPHA2*, are functionally important for LNEP migration. Activated LNEPs treated with AXL- and EPHA2-specific inhibitors (3 μM R428 and 1 μM ALW-II-247) show compromised motility in wound closure assays. Relative wound area at 24 h as compared with 0 h is graphed as mean ± s.e.m. from $n = 3$ independent experiments. *P* values were derived by unpaired two-tailed Student's *t*-test. (**d**) Schematic summary of a common, hypoxia-mediated epithelial progenitor response. Following major lung injury, local hypoxia promotes Notch signalling and a Krt5^{pos} remodelling program in quiescent p63^{pos} LNEPs via HIF1α, leading to robust migration, squamous metaplasia, and the ultimate formation of dysplastic alveolar barriers. However, Wnt activity prior to Krt5 activation favours p63^{neg} LNEP expansion and differentiation toward AEC2s, leading to normal alveolar epithelial repair. The appearance of Krt5^{pos}/SPC^{pos} cells in several human disease/injury settings further suggests an intermediate response that may result in concurrent dysplastic and appropriate alveolar repair.

delivery. Injury-induced loss of alveolar epithelium leads to alveolar collapse, disrupting critical gas exchange and producing local hypoxia as oxygenated blood is diverted from non-ventilated areas[33]. Regeneration from such injury represents a major challenge given the necessity to reconstitute effective barriers over such a large area. Nonetheless, as judged by the extensive expansion of epithelial progenitor cells throughout the alveoli of flu-injured mouse lungs[2,6,7] and diversely injured human lungs (Fig. 5a–c), the alveolar epithelium is remarkably regenerative. Whether this regenerative process results in normal or dysplastic repair, however, is dependent on several signalling pathways, and we can now provide additional insights into this process. First, we identify hypoxia itself as a key driver of Notch signalling critical to activation epithelial stem/progenitor cells (Figs 3, 6 and 7d). Hypoxia has been previously reported to induce Notch activity *in vitro*[34,35], and we now provide *in vivo* evidence that hypoxia drives Notch activity because HIF1α is essential for NICD DNA binding under hypoxic conditions (Fig. 3g and Supplementary Fig. 3d). Secondly, we find that hypoxia/Notch-activated progenitors in both mice and humans upregulate a common set of genes regulating motility and invasion (Fig. 7). Live imaging confirms that activated LNEPs are highly motile within injured lung[2] as well as in *in vitro* migration assays (Fig. 7). This phenotype is probably fitted to the migration across large distances through fibrinous environments required for reconstitution of alveolar barriers. That this process in

lung epithelia is hypoxia driven despite the improved outcome with enhanced AEC2 expansion (Fig. 1h–j) underscores the fundamental nature of HIF1α-dependent cellular responses to acute hypoxia in all cells and its overall protective effect on survival[36]. Finally, we demonstrate that activation of Wnt or suppression of HIF1α signalling further empowers non-AEC2 progenitors (Sox2^{pos} p63^{neg} LNEPs) to contribute to AEC2 recovery and improved lung function. Collectively, these findings highlight both the potential and the signals directing alveolar regenerative programs centred on activation of epithelial progenitors in distal airways.

The ultimate fate of p63^{neg} and p63^{pos} LNEPs appears dependent on both Notch and Wnt signals not only at the level of single-cell differentiation but also at the level of amplification of fated cells by the same signals directing their initial commitment. Thus, *in vivo* expansion of AEC2s from Sox2^{pos} cells with HIF1α deletion or stabilized β-catenin (Figs 2a and 4a) reflects both an initial state change for p63^{neg} LNEPs resulting in SPC^{pos} cells and their subsequent expansion into the injured parenchyma. Likewise, p63^{pos} LNEPs are the major responders to HIF1α/Notch signals producing the entire Krt5^{pos} response (Fig. 1a), whereas Wnt suppresses this pathway in favour of p63^{neg} LNEP-derived AEC2s (Fig. 4a). The overall outcome of basal-like metaplasia or AEC2 regeneration is largely determined by which pathway dominates the competitive selection between these populations after an initial fate choice, as indicated schematically in Fig. 7d. While Sox2^{pos} LNEPs are clearly an important contributor to AEC2 regeneration, surviving AEC2s are also proliferative (Fig. 2d) and doubtless participate in alveolar repair[1,9,37].

Whereas in mice only rare p63^{pos} LNEPs account for dramatic Krt5^{pos} expansion after influenza (Fig. 1a), human alveoli, after both acute and chronic injury, are re-populated by Krt5^{pos} expansion of several cell types: SPC^{pos}/Krt5^{pos} alveolar cells as well as p63^{pos} LNEP homologues and p63^{pos}/Krt5^{pos} classical basal cells, both prominent in distal human airways[2,38]. Human AEC2s appear more plastic than their murine counterparts as, unlike in mice, human AEC2s rapidly lose *SFTPC* and express Notch-driven *KRT5* when cultured (Supplementary Fig. 7d). Nonetheless, our studies in mice suggest that human lungs may also face the conundrum that, once established after major injury, neither removal of Notch signalling nor Wnt stimulation reverses differentiation down the Krt5 pathway (Supplementary Fig. 5), contributing to a poor functional outcome. It also remains unknown whether there is a true p63^{neg} LNEP in distal human airways capable of contributing to normal alveolar repair. Future studies in humans are needed to both further define the potential for airway progenitors to mobilize a regenerative alveolar program and to elucidate the micro-environmental conditions that favour predominantly AEC2 expansion. □

METHODS

Methods, including statements of data availability and any associated accession codes and references, are available in the online version of this paper.

Note: Supplementary Information is available in the online version of the paper

ACKNOWLEDGEMENTS

This work was supported by NIH grants RO1 HL128484, UO1 HL111054, UO1 134766, and a sponsored research agreement with Biogen Idec (H.A.C.). A.E.V. was supported by T32 HL007185-36, F32 HL117600-01, and K99 HL131817. M.A.M. and J.E.G. were supported by NHLBI grant R37HL51856 and R37HL57156. J.X. was supported by NIH grants R01 CA112403 and R01 CA193455 and CPRIT grants RP120732-P5 and RP150197. J.M.S. was supported by NIH grant R01 HL084376. We thank M.A.M. and P. Wolters at the UCSF Interstitial Lung Disease Blood and Tissue Repository for procuring non-donor and diseased lung tissues, respectively. We also thank J.E.G. for providing influenza PR8 virus and technical assistance, B. Sennino for hypoxyprobe and technical advice, M. Zhang for CHIR99021 and technical advice, R. Lao of the Institute for Human Genetics core facility, UCSF, for assistance with RNA-sequencing, and D. A. Denison and S. Zaki of the CDC for lung tissue slides obtained from patients with H1N1 influenza.

AUTHOR CONTRIBUTIONS

Conceptualization: Y.X., H.A.C., A.E.V.; investigation: Y.X., T.K., A.N.B., J.X., D.-K.L., Y.W., V.T., J.R.J., J.M.S., H.A.C., J.E.G., M.A.M., A.E.V.; formal analysis: Y.X., I.H.D., A.E.V.; writing: Y.X., H.A.C., A.E.V.; supervision: H.A.C.; funding acquisition: H.A.C., A.E.V.

COMPETING FINANCIAL INTERESTS

The authors declare no competing financial interests.

Published online at http://dx.doi.org/10.1038/ncb3580

1. Desai, T. J., Brownfield, D. G. & Krasnow, M. A. Alveolar progenitor and stem cells in lung development, renewal and cancer. *Nature* **507,** 190–194 (2014).
2. Vaughan, A. E. *et al.* Lineage-negative progenitors mobilize to regenerate lung epithelium after major injury. *Nature* **517,** 621–625 (2015).
3. Rawlins, E. L. *et al.* The role of Scgb1a1+ Clara cells in the long-term maintenance and repair of lung airway, but not alveolar, epithelium. *Cell Stem Cell* **4,** 525–534 (2009).
4. Tata, P. R. *et al.* Dedifferentiation of committed epithelial cells into stem cells *in vivo*. *Nature* **503,** 218–223 (2013).
5. Hogan, B. L. *et al.* Repair and regeneration of the respiratory system: complexity, plasticity, and mechanisms of lung stem cell function. *Cell Stem Cell* **15,** 123–138 (2014).
6. Kumar, P. A. *et al.* Distal airway stem cells yield alveoli in vitro and during lung regeneration following H1N1 influenza infection. *Cell* **147,** 525–538 (2011).
7. Zuo, W. *et al.* p63^{+}Krt5^{+} distal airway stem cells are essential for lung regeneration. *Nature* **517,** 616–620 (2015).
8. Guseh, J. S. *et al.* Notch signaling promotes airway mucous metaplasia and inhibits alveolar development. *Development* **136,** 1751–1759 (2009).
9. Barkauskas, C. E. *et al.* Type 2 alveolar cells are stem cells in adult lung. *J. Clin. Invest.* **123,** 3025–3036 (2013).
10. Loosli, C. G. *et al.* The destruction of type 2 pneumocytes by airborne influenza PR8-A virus; its effect on surfactant and lecithin content of the pneumonic lesions of mice. *Chest* **67,** 7S–14S (1975).
11. Ray, S. *et al.* Rare SOX2+ airway progenitor cells generate KRT5+ cells that repopulate damaged alveolar parenchyma following influenza virus infection. *Stem Cell Rep.* **7,** 817–825 (2016).
12. Gerovac, B. J. *et al.* Submersion and hypoxia inhibit ciliated cell differentiation in a notch-dependent manner. *Am. J. Respir. Cell Mol. Biol.* **51,** 516–525 (2014).
13. Dang, T. P., Eichenberger, S., Gonzalez, A., Olson, S. & Carbone, D. P. Constitutive activation of Notch3 inhibits terminal epithelial differentiation in lungs of transgenic mice. *Oncogene* **22,** 1988–1997 (2003).
14. Tsao, P.-N. *et al.* γ-secretase activation of notch signaling regulates the balance of proximal and distal fates in progenitor cells of the developing lung. *J. Biol. Chem.* **283,** 29532–29544 (2008).
15. Pardo-Saganta, A. *et al.* Parent stem cells can serve as niches for their daughter cells. *Nature* **523,** 597–601 (2015).
16. Lafkas, D. *et al.* Therapeutic antibodies reveal Notch control of transdifferentiation in the adult lung. *Nature* **528,** 127–131 (2015).
17. Morimoto, M., Nishinakamura, R., Saga, Y. & Kopan, R. Different assemblies of Notch receptors coordinate the distribution of the major bronchial Clara, ciliated and neuroendocrine cells. *Development* **139,** 4365–4373 (2012).
18. Mucenski, M. L. *et al.* β-Catenin is required for specification of proximal/distal cell fate during lung morphogenesis. *J. Biol. Chem.* **278,** 40231–40238 (2003).
19. Okubo, T. & Hogan, B. L. Hyperactive Wnt signaling changes the developmental potential of embryonic lung endoderm. *J. Biol.* **3,** 11 (2004).
20. Hashimoto, S. *et al.* β-Catenin-SOX2 signaling regulates the fate of developing airway epithelium. *J. Cell Sci.* **125,** 932–942 (2012).
21. Frank, D. B. *et al.* Emergence of a wave of Wnt signaling that regulates lung alveologenesis by controlling epithelial self-renewal and differentiation. *Cell Rep.* **17,** 2312–2325 (2016).
22. Guha, A. *et al.* Neuroepithelial body microenvironment is a niche for a distinct subset of Clara-like precursors in the developing airways. *Proc. Natl Acad. Sci. USA* **109,** 12592–12597 (2012).

23. Cai, Y. *et al*. Transgenically-expressed secretoglobin 3A2 accelerates resolution of bleomycin-induced pulmonary fibrosis in mice. *BMC Pulm. Med.* **15,** 72 (2015).
24. Reynolds, S. D. *et al*. Conditional stabilization of β-catenin expands the pool of lung stem cells. *Stem Cells* **26,** 1337–1346 (2008).
25. Tzouvelekis, A. *et al*. Comparative expression profiling in pulmonary fibrosis suggests a role of hypoxia-inducible factor-1alpha in disease pathogenesis. *Am. J. Respir. Crit. Care Med.* **176,** 1108–1119 (2007).
26. Bodempudi, V. *et al*. miR-210 promotes IPF fibroblast proliferation in response to hypoxia. *Am. J. Physiol. Lung Cell. Mol. Physiol.* **307,** L283–L294 (2014).
27. Gonzalez, R. F., Allen, L., Gonzales, L., Ballard, P. L. & Dobbs, L. G. HTII-280, a biomarker specific to the apical plasma membrane of human lung alveolar type II cells. *J. Histochem. Cytochem.* **58,** 891–901 (2010).
28. Jarriault, S. *et al*. Signalling downstream of activated mammalian Notch. *Nature* **377,** 355–358 (1995).
29. Chen, X. *et al*. XBP1 promotes triple-negative breast cancer by controlling the HIF1alpha pathway. *Nature* **508,** 103–107 (2014).
30. Chi, J. T. *et al*. Gene expression programs in response to hypoxia: cell type specificity and prognostic significance in human cancers. *PLoS Med.* **3,** e47 (2006).
31. Holland, S. J. *et al*. R428, a selective small molecule inhibitor of Axl kinase, blocks tumor spread and prolongs survival in models of metastatic breast cancer. *Cancer Res.* **70,** 1544–1554 (2010).
32. Amato, K. R. *et al*. Genetic and pharmacologic inhibition of EPHA2 promotes apoptosis in NSCLC. *J. Clin. Invest.* **124,** 2037–2049 (2014).
33. Sommer, N., Strielkov, I., Pak, O. & Weissmann, N. Oxygen sensing and signal transduction in hypoxic pulmonary vasoconstriction. *Eur. Respir. J.* **47,** 288–303 (2015).
34. Gustafsson, M. V. *et al*. Hypoxia requires notch signaling to maintain the undifferentiated cell state. *Dev. Cell* **9,** 617–628 (2005).
35. Sahlgren, C., Gustafsson, M. V., Jin, S., Poellinger, L. & Lendahl, U. Notch signaling mediates hypoxia-induced tumor cell migration and invasion. *Proc. Natl Acad. Sci. USA* **105,** 6392–6397 (2008).
36. Iyer, N. V. *et al*. Cellular and developmental control of O2 homeostasis by hypoxia-inducible factor 1α. *Genes Dev.* **12,** 149–162 (1998).
37. Evans, M. J., Cabral, L. J., Stephens, R. J. & Freeman, G. Transformation of alveolar Type 2 cells to Type 1 cells following exposure to NO2. *Exp. Mol. Pathol.* **22,** 142–150 (1975).
38. Rock, J. R. *et al*. Basal cells as stem cells of the mouse trachea and human airway epithelium. *Proc. Natl Acad. Sci. USA* **106,** 12771–12775 (2009).

METHODS

Animals and treatment All animal procedures were approved by the Institutional Animal Care and Use Committee of UCSF and all animal experiments were done in compliance with ethical guidelines and the approved protocols. *HIF1α*$^{fl/fl}$ (ref. 39), Shh-Cre (ref. 40), Krt5-CreERT2 (ref. 41), Sox2-CreERT2 (ref. 42), β-catenin^{loxEx3} (ref. 43), CC10-CreERT (ref. 44), FoxJ1-CreERT2 (ref. 45), p63-CreERT2 (ref. 46), Ub-GFP (ref. 47), SPC-CreERT2 (ref. 48), and Ai14-tdTomato (ref. 49) mice were previously described. For all experiments, 6–8-week-old animals of both sexes were used in equal proportions. All animal studies utilized a minimum of 3 mice per group.

For influenza infection, mice were administered 280 FFU of Influenza H1N1 (PR8) intranasally (survival rate >90%). Briefly, PR8 virus dissolved in 30 µl of PBS was pipetted onto the nostrils of heavily anesthetized mice (agonal breathing), whereupon mice aspirated the fluid directly into their lungs.

For all animal studies, no statistical method was used to predetermine sample size. The experiments were not randomized, and the investigators were not blinded to allocation during experiments and outcome assessment.

Lineage tracing. For analysing the lineage fate of Sox2-expressing cells, a single dose of 0.25 mg g^{-1} body weight tamoxifen dissolved in 50 µl corn oil was administered i.p. one week before PR8 infection. For HIF1α deletion in Sox2^{+} cells, three doses of tamoxifen were utilized to ensure complete deletion. To trace Krt5^{pos} cells, a single dose of 0.125 mg g^{-1} tamoxifen was administered i.p. at day 7 to 10 post-PR8 infection when Krt5^{pos} cells were abundant. To purify LNEPs by excluding club cells and multi-ciliated cells, five doses of 0.25 mg g^{-1} body weight tamoxifen were administered to CC10-CreERT; FOXJ1-CreERT2; Ai14-tdTomato mice i.p. two weeks before euthanizing the mice to maximize the recombination. To determine the cell of origin for post-influenza Krt5^{+} cells, p63-CreERT2/tdTomato mice were administered five doses of 0.25 mg g^{-1} body weight tamoxifen. We waited 6 weeks for tamoxifen clearance and then infected as described above. Background (tamoxifen-independent) recombination in p63-CreERT2 mice is <1%.

Tissue hypoxia detection To detect hypoxic regions in tissue, mice received pimonidazole hydrochloride (60 mg kg^{-1} body weight, i.p., Hypoxyprobe Plus kit) 1 h before euthanization. The lungs were inflated with 1% paraformaldehyde (PFA), incubated with 30% sucrose overnight and embedded with OCT. Sections (80 µm thick) were cut and air-dried overnight on Superfrost plus slides (Fisher Scientific). The sections were stained with FITC-conjugated anti-pimonidazole mouse IgG (1:100, 4.3.11.3 mouse FITC-MAb, Hypoxyprobe Plus kit) together with rabbit anti-Krt5 (1:1,000; Covance, no. PRB-160P) overnight in PBS plus 1% BSA, 5% nonimmune horse serum (UCSF Cell Culture Facility), 0.3% Triton X-100 (Sigma), and 0.02% sodium azide (Sigma), followed by secondary antibody and DAPI staining. The slides were mounted with Prolong (Invitrogen) and imaged with a Yokogawa spinning-disk confocal (UCSF Biological Imaging Development Center).

Saturated phosphatidylcholine (SatPC) measurement SatPC was isolated from lungs of newborn animals. Lungs were first weighed, then placed in ice-cold 0.9% saline and pulse sonicated. Total lipids were extracted as previously described (ref. 50). SatPC was isolated as previously described (ref. 51) and normalized to lung weight.

Pulse oximetry. Arterial oxygen saturation was measured using the MOUSEOX Pulse Oximeter system (Starr Life Science). Mice were shaved prior to infection and the CollarClip utilized so that measurements could be taken without anesthesia. Measurements were taken for at least 3 min per mouse after establishing the first successful reading. Error-free measurements were then averaged for each time point for each mouse.

Excess lung water analysis. This analysis was performed as previously described[52]. Briefly, the lungs were removed, weighed and homogenized (after addition of 1 ml distilled water). The blood was collected through right-ventricle puncture. The homogenate was weighed and a fraction was centrifuged (10,000*g*, 8 min) for assay of haemoglobin concentration in the supernatant. Another fraction of homogenate, supernatant, and blood were weighed and then desiccated in an oven (60 °C for 24 h). Calculations of water fraction, blood volume, water volume, whole lung dry weight, and ultimately excess lung water calculations were performed using equations previously described[52]. The mice used for this analysis were the same cohort used for pulse oximetry.

Tissue preparation and immunofluorescence (IF) Freshly dissected mouse lungs were inflated with 4% PFA plus 50% OCT dissolved in PBS for 1 h at room temperature. After fixation, the lungs were washed with PBS and incubated with 30% sucrose plus 50% OCT overnight, then embedded in OCT and frozen the following day. Cryosections (7 µm thick) were cut and fixed for an additional 5 min in 4% PFA at room temperature, then incubated with 0.1% sodium borohydride (Sigma-Aldrich) in PBS to reduce aldehyde-induced background fluorescence for 3 × 10-min intervals, and subsequently blocked and stained in PBS plus 1% BSA (Affymetrix), 5% nonimmune horse serum, 0.1% Triton X-100, and 0.02% sodium azide.

Cells spun on slides were fixed with 4% PFA for 5 min before cytospin and then stained as above. Cell grown on Matrigel were fixed in IHC Zinc Fixative (BD) for 5 min and subsequently blocked and stained in TBS-based blocking buffer, as the zinc fixative reacts with phosphate.

The following antibodies were used for IF: rabbit anti-pro-SPC (1:3,000; Millipore, no. AB3786), goat anti-pro-SPC (1:2,000; Santa Cruz, no. SC-7706), rabbit anti-Krt5 (1:1,000; Covance, no. PRB-160P), chicken anti-Krt5 (1:1,000; Covance, no. SIG-3475), rabbit anti-ΔNp63 (1:100; Cell Signaling, no. 13109), rat anti-mouse integrin β4 (1:200; BD, no. 555721), goat anti-CC10 (1:10,000, a gift from B. Stripp, Cedars-Sinai Medical Center, USA), mouse anti-acetylated tubulin (1:500, Sigma, 6-11B-1), rat anti-E-cadherin (1:500, Invitrogen, no. 13-1900), rabbit anti-Hes1 (1:1,000; Cell Signaling, no. 11988), goat anti-Scgb3a2 (1:100, R&D, AF3465).

Quantification of immunofluorescence. To quantify Krt5^{pos} or AEC2-depleted area, mosaic images covering the whole lobes were generated from multiple ×10 fields captured on a Zeiss AxioImager upright fluorescent microscope and tiled using 10% image overlap by Axiovision 4.7 software. The Krt5^{pos} or SPC^{pos} areas and total areas were measured using outline spline in the measure menu of Axiovision 4.7. At least 3 sections, each section containing 2–3 individual lobes and separated by over 300-µm depth were quantified for each mouse ($n \geq 5$ mice).

To lineage trace Sox2-expressing cells into alveolar cell fate, all the traced cells in injured alveolar area were captured at ×20 magnification and counted using events in the measure menu of Axiovision 4.7. On average, >3,000 cells were counted per section. For each mouse, we quantified at least 2 sections, each containing 2–3 individual lobes and separated by over 300-µm depth ($n \geq 4$ mice).

To quantify p63-CreERT2 trace of Krt5^{+} cells post-influenza, images were captured as above and cells were counted from >4 sections per mouse and included at least 3 individual lobes. In total, >3,200 cells were scored from $n = 3$ mice.

To quantify Krt5^{pos} or SPC^{pos} cell percentage in cultured LNEPs accurately, the colonies were dissociated from Matrigel and digested into single-cell suspension as described below, followed by cytospin and staining. Stained cells were captured at ×20 and at least 600 cells were counted per condition.

Mouse lung epithelial cell isolation and flow cytometry. Mouse lung epithelial cells were isolated as previously described[2]. For FACS analysis, single-cell preparations were negatively selected with biotinylated antibodies: rat anti-mouse CD45 (1:200, BD, no. 553078), rat anti-mouse CD16/CD32 (1:200, BD, no. 553143), rat anti-mouse CD31 (1:200, BD, no. 553371), and then incubated for 1 h at 4 °C with the following primary antibodies or viability dye diluted in DMEM (without phenol red) plus 2% FBS (Gibco): phycoerythrin (PE) or BV421-conjugated rat anti-mouse EpCAM (1:500; Biolegend, no. 563477, no. 563214), Alexa Fluor 647 or PE-conjugated rat anti-mouse integrin β4 (1:75; BD, no. 553745), fixable viability dye eFluor 780 (1:2,000, eBioscience). Sorting and analysis was performed on BD FACS Aria cytometers. Of note, so far we do not have a method to isolate completely pure LNEPs. For culture, we used EpCAM^{pos}β4^{pos} cells, which have a contamination of club cells and multi-ciliated cells, but the contaminated cells do not grow in culture. To isolate highly purified LNEPs, we used CC10/FOXJ1 double Cre mice to exclude club and multi-ciliated cells, leading to similar results as the method we developed in a previous study using CD14 and CD200 antibodies[2].

For intracellular flow, single-cell preparations were negatively selected and stained with eFluor 780 as above, then fixed with IHC Zinc Fixative (BD) for 30 min at 4 °C, permeabilized with PBS pH 7.2, 0.1% bovine serum albumin (BSA), 0.2% saponin for 5 min, and stained with primary and secondary antibodies in permeabilization buffer sequentially. Goat anti-pro-SPC (1:500; Santa Cruz, no. SC-7706), BV421 rat anti-mouse EpCAM, and Alexa Fluor 488 donkey anti-goat IgG (1:2,000, ThermoFisher, no. A-11055) were used.

Cell line identity. No cell lines were used in this study.

Mouse LNEPs culture. Mouse lung LNEPs were flow sorted by EpCAM^{pos}β4^{pos} and cultured on Matrigel (BD) as follows. A 48-well plate or 8-well chamber slide was coated with 150 µl Matrigel per well, allowed to solidify at 37 °C, and then equilibrated with SABM (Lonza) for at least 30 min prior to cell plating. A total of 15,000 to 25,000 cells were plated in each well and maintained in SAGM (Lonza) supplemented with 5% charcoal-stripped FBS (ThermoFisher), 10 ng ml^{-1} KGF (FGF-7, Peprotech), 10 µM Y-27632 (Sigma) and 50 ng ml^{-1} murine noggin (Peprotech) for the first 2 days, and then replaced with SAGM supplemented with 5% charcoal-stripped FBS and 10 ng ml^{-1} KGF with or without CHIR99021 (2 nM dissolved in dimethylsulfoxide (DMSO)) for an additional 5–7 days. Cells were passed once a week by incubation with 25 U ml^{-1} Dispase II (Roche) at 37 °C for

DOI: 10.1038/ncb3580

20 min to liberate colonies and followed by 15 min incubation with 2 mM EDTA in PBS at 37 °C to dissociate the colonies and obtain a single-cell suspension. The cells were then plated on Matrigel and maintained in SAGM supplemented with 5% charcoal-stripped FBS and 10 ng ml^{-1} KGF with or without CHIR99021 through additional passages. Cells were gradually activated (expressed Krt5) over time in culture, as described in the manuscript.

For air/liquid interface experiments, mouse LNEPs were isolated as described above and grown for a single passage in submersion conditions to establish the culture. Cells were then liberated and replated into continued Matrigel submersion culture or on Matrigel layered on top of a Transwell membrane exposed to air (COSTAR Transwell Permeable Support, no. 3413), cultured for 7 days, and then isolated as above for RNA. For hypoxyprobe staining, 2 μM pimonidazole was added to culture media in each condition for 1 h on the seventh day after seeing. Cells were then washed thoroughly with TBS before zinc fixation and stained as described above.

For LNEP isolation from p63-CreERT2/tdTomato mice, mice were treated with 5 doses of tamoxifen, and EpCAM^{pos}β4^{pos} cells were flow sorted and cultured as normal. Wells were visually inspected to confirm that cultures only rarely contained endogenous p63-labelled (tdTomato^{+}) cells. Labelling was induced by a 24 h pulse of 100 nM hydroxytamoxifen (4OHT) 24 h after re-plating for the second passage (~10 days after isolation), demonstrating induction of p63 expression in cells that were p63^{neg} *in situ* (see Supplementary Fig. 4d).

Migration assay. Transwell assays were performed with Corning BioCoat Invasion Chambers (inserts coated with Matrigel, 8.0 μm pore size). Primary human basal-enriched and AEC2s (80,000 and 200,000 respectively) were seeded on top of the inserts in SAGM with KGF, Noggin and Y-27632 for 2–3 days for recovery, then washed with PBS and starved with SABM for 6 h before migration through Matrigel toward 1% FBS plus 50 ng ml^{-1} EGF in SAGM at 37 °C for ~66 h (with SABM on top of the inserts). Non-invaded cells and Matrigel were removed by swabbing. Invaded cells were fixed in methanol, stained with 1% crystal violet (Sigma-Aldrich), and imaged with a Zeiss AxioImager at ×10 magnification. Invaded cells were counted in random fields avoiding the edge of the insert.

Wound closure assays were performed using specific culture inserts (Ibidi, no. 80209). A culture insert was transferred to an individual well of a 24-well plate and the surface in the insert was coated with 1:20 diluted Matrigel for 2 h before cell seeding. Activated LNEPs were disaggregated as described above and resuspended in SAGM with KGF, Noggin and Y-27632 at a density of 0.7–1 million ml^{-1}. Seventy microlitres of cell suspension was seeded into each well of the insert. After cell attachment for about 24 h forming a confluent layer, the cells were pretreated with inhibitors for 1 h before removing the culture inserts, and then washed with PBS twice and incubated with fresh SAGM medium in the presence/absence of the AXL inhibitor R428 (Apexbio) or the EPHA2 inhibitor ALW-II-41-27 (Apexbio) dissolved in DMSO. The cell migration into the defined cell-free gap (500 μm) was observed for 24 h under an inverted microscope (Nikon). Images of the cell-free gap were captured at 0 h and 24 h, and total cell-free area was quantified with Axiovision 4.7.

Chromatin immunoprecipitation (ChIP). ChIP experiments were performed following the Imprint Chromatin Immuno-precipitation protocol (Sigma). Expanded LNEP colonies were digested as described above, seeded on 1:20 diluted Matrigel-coated 10 cm dishes and harvested on reaching 80–90% confluence. Cells were crosslinked with 4% formaldehyde for 10 min followed by nuclei isolation, sonication to shear DNA into 100–500 bp fragments, protein/DNA complex pulldown and crosslink reversal. One microgram of rabbit anti-Cleaved Notch1 (Cell Signaling, no. 4147) and goat anti-HIF1α (R&D Systems, no. AF1935) antibody were used for each IP. The precipitated DNA and input DNA was quantified by qPCR using specific primers on Krt5, Hey1 and Hes5 promoters.

Human tissues. All human normal and fibrotic tissue samples were obtained from UCSF Interstitial Lung Disease Blood and Tissue Repository and are classified as Non-identifiable Otherwise Discarded Human Tissues, for which no consent/IRB approval is required. Slides from lung tissue blocks of non-identified human subjects with documented H1N1 influenza A infection 10–21 days after diagnosis and without secondary bacterial infection, as judged by PCR screening, were obtained from A. Denison at the Center for Disease Control (Atlanta).

Human lung epithelial cell isolation. Distal lung tissue was obtained and dissected into roughly 5 cm^3 pieces. Tissue was washed in 500 ml sterile PBS for 10 min at 4 °C at least two times, or until PBS no longer appeared obviously bloody. An additional 10 min wash was then performed with Hank's buffered saline solution (HBSS). Using autoclaved Kim Wipes, tissue was compressed to remove as much liquid as possible and further dissected into 1 cm^3 pieces. Sterile HBSS buffer containing 5 U ml^{-1} Dispase II and 0.1 mg ml^{-1} DNase I^{+} penicillin/streptomycin was added to the small tissue pieces. Tissue rapidly takes up the digest solution at this point, becoming visibly engorged. Tissue was digested for 2 h at 37 °C and Fungizone (1:400) was added for the final 30 min of the digest. The digest solution was then stored overnight at 4 °C without further degradation of cells due to lack of Dispase activity at this temperature. The following day, the tissue in digestion solution was warmed to 37 °C and liquefied using an Osterizer 12 Speed Blender as follows: 5 s pulse, 5 s grate, and 2–5 s pulse. The suspension was poured through a glass funnel lined with sterile 4 × 4 gauze, applying some compression to recover as much of the solution as possible. The cell suspension was sequentially filtered through 100 μm, 70 μm and 40 μm strainers. Finally, red blood cells were removed using Red Blood Cell Lysis Buffer (Sigma-Aldrich).

Single-cell RNA-Seq of human lungs. The cell preparations were stained as described for mouse cells with corresponding anti-human antibodies: HTII-280 (1:100, a generous gift from L. Dobbs, University of California - San Francisco, USA), anti-human/mouse CD49f (1:100, Biolegend, no. 313602), PE anti-human EpCAM (1:400, Biolegend, no. 324206), and anti-human CD45 APC-Cy7 (1:200, Biolegend, no. 304014). As judged by cytospin, all the SPC^{pos} cells were captured by HTII-280 sort. Sorted single cells were captured on a small-sized (7–10 μm cell diameter) microfluidic mRNA seq chip (Fluidigm) using the Fluidigm C1 Single-Cell Auto Prep System. The downstream steps (lysis, cDNA synthesis/amplification, library preparation) were carried out following the Fluidigm C1 protocol, incorporating the Illumina Nextera XT DNA Sample Preparation Kit. Nextera libraries consisting of barcoded single-cell samples were pooled and sequenced on an Illumina HiSeq 2,500 sequencer using high-output mode with 100 bp paired-end reads. This results in a sequencing depth of ~2–3 million reads per single-cell sample. Paired-end fastq files were aligned using the Tophat/Bowtie2 software[53] and annotated using the Cufflinks package[54] and the UCSC hg19 index (Illumina), followed by normalization using Cuffnorm. Cells with a fragment mapping rate below 50% and less than 1,000 genes sequenced (1 FPKM threshold) were filtered out. Genes that were not expressed at 1 FPKM in at least 3 cells were also removed prior to subsequent Fluidigm Singular analysis running in R, leading to ~13,000 genes. We successfully sequenced a total of 72 AEC2s and 23 basal-enriched cells from a normal lung, 49 AEC2s from scleroderma, 48 AEC2s from dyskeratosis congenita, and 27 AEC2s from IPF lung. Differential expression analysis from Singular is included in Supplementary Tables 1,3–6. Ingenuity pathway analysis (IPA, QIAGEN, www.qiagen.com/ingenuity) was performed on this differential expression data and is found in Supplementary Tables 2, 7–9.

RNA-Seq of mouse normal and activated LNEPs. Highly purified quiescent LNEPs (EpCAM^{pos}β4^{pos}CC10^{neg}FoxJ1^{neg}) and activated LNEPs (Krt5-CreERT2 traced cells 17 days post infection) were flow sorted and RNA extracted using ReliaPrep RNA Tissue Miniprep kit (Promega). cDNA synthesis/amplification, library preparation and sequencing followed the same protocol used in Single Cell RNA-Seq.

Western blot analysis. Snap-frozen mouse lungs were ground into tissue powder and then lysed in the RIPA buffer (50 mM Tris-HCl, pH 7.5, 150 mM NaCl, 1% deoxycholate, 0.1% SDS, 1% Triton X-100) supplemented with Protease Inhibitor Cocktail, 1 mM phenylmethyl sulfonyl fluoride, 1 mM sodium vanadate, 10 mM sodium fluoride, and Phosphatase Inhibitor Cocktail. The lysates were quantified using Pierce BCA protein assay kit (Thermo, no. 23225), normalized and blotted for HIF1α (1:500, R&D Systems, no. AF1935), pro-SPC (1:500, Millipore, no. AB3786), Krt5 (1:1,000, Covance, no. PRB-160P), Cleaved Notch1 (1:1,000, Cell Signaling, no. 4147), E-cadherin (1:2,000, BD, no. 610181), β-actin (1:10,000, Sigma-Aldrich, no. A5441). To detect influenza A virus, unboiled lysates in 1 mM dithiothreitol and 2% SDS were blotted with anti-Influenza A antibody (1:1,000, Millipore, no. AB1074).

Bronchoalveolar lavage. After the trachea was exposed, a 20-G catheter was inserted into the trachea for lavage. Cold PBS (1 ml) was instilled into the mouse lungs followed by gentle aspiration repeated three times. All of the bronchoalveolar lavage fluid was centrifuged and the supernatant was collected to measure total protein content using BCA assay. The cell pellet was resuspended in Red Blood Lysis Buffer and counted using a haemocytometer.

Colony-formation assay. Ten thousand freshly sorted or cultured single LNEPs were plated onto a Matrigel-coated 8-well chamber slide and cultured for one week. Colonies were fixed with IHC Zinc Fixative and stained. Only colonies containing more than 5 nuclei were counted.

qRT-PCR analysis. Snap-frozen lungs were ground into tissue powder and RNA was isolated using the ReliaPrep RNA Tissue Miniprep kit (Promega). ReliaPrep RNA Cell Miniprep kit (Promega) was used to isolate RNA from freshly sorted cells or cultured cells. To isolate RNA from cultured LNEPs on Matrigel, colonies were dissociated from Matrigel using Dispase II first, and then the cell pellets were lysed following the Promega protocol. cDNA was synthesized using Superscript III (Invitrogen)

and assayed for gene expression using Faststart Universal SYBR green Master Mix (Roche). PCR reaction and analysis was run on Eppendorf Mastercycler ep realplex 2. HPRT, L19 and GAPDH were used as internal controls and all of the data were normalized by L19. All primer sequences are as listed in Supplementary Table 10.

Statistics and reproducibility. For single-cell RNA-Seq analysis, Fluidigm Singular software was used. All other statistical calculations were performed using Graphpad Prism. Variance for all group data is expressed as ±s.e.m. The statistical test used to determine significance for each experiment is stated in the corresponding figure legend. A *P* value less than 0.05 was accepted as significant. The investigators were not blinded to allocation during experiments and outcome assessment. All images are representative of at least three independent experiments or mice of the same genotype. Western blots are representative of multiple independent experiments, and unprocessed original scans of blots are displayed in Supplementary Fig. 8. No statistical method was used to predetermine sample size and experiments were not randomized. All experiments presented were reproducible and *n* for each experiment is presented in each figure legend.

Data availability. RNA-Seq data that support the findings of this study have been deposited in the Gene Expression Omnibus (GEO) under accession codes GSE83467 and GSE83501. Source data for the main and supplementary figures have been provided as Supplementary Table 11. All other data supporting the findings of this study are available from the corresponding author on reasonable request.

39. Ryan, H. E. *et al.* Hypoxia-inducible factor-1alpha is a positive factor in solid tumor growth. *Cancer Res.* **60,** 4010–4015 (2000).
40. Harfe, B. D. *et al.* Evidence for an expansion-based temporal Shh gradient in specifying vertebrate digit identities. *Cell* **118,** 517–528 (2004).
41. Van Keymeulen, A. *et al.* Distinct stem cells contribute to mammary gland development and maintenance. *Nature* **479,** 189–193 (2011).
42. Arnold, K. *et al.* Sox2(+) adult stem and progenitor cells are important for tissue regeneration and survival of mice. *Cell Stem Cell* **9,** 317–329 (2011).
43. Harada, N. *et al.* Intestinal polyposis in mice with a dominant stable mutation of the β-catenin gene. *EMBO J.* **18,** 5931–5942 (1999).
44. Rawlins, E. L. *et al.* The role of Scgb1a1+ Clara cells in the long-term maintenance and repair of lung airway, but not alveolar, epithelium. *Cell Stem Cell* **4,** 525–534 (2009).
45. Rawlins, E. L., Ostrowski, L. E., Randell, S. H. & Hogan, B. L. Lung development and repair: contribution of the ciliated lineage. *Proc. Natl Acad. Sci. USA* **104,** 410–417 (2007).
46. Lee, D.-K., Liu, Y., Liao, L., Wang, F. & Xu, J. The prostate basal cell (BC) heterogeneity and the p63-positive BC differentiation spectrum in mice. *Int. J. Biol. Sci.* **10,** 1007–1017 (2014).
47. Schaefer, B. C., Schaefer, M. L., Kappler, J. W., Marrack, P. & Kedl, R. M. Observation of antigen-dependent CD8+ T-cell/ dendritic cell interactions *in vivo*. *Cell. Immunol.* **214,** 110–122 (2001).
48. Chapman, H. A. *et al.* Integrin α6β4 identifies an adult distal lung epithelial population with regenerative potential in mice. *J. Clin. Invest.* **121,** 2855–2862 (2011).
49. Madisen, L. *et al.* A robust and high-throughput Cre reporting and characterization system for the whole mouse brain. *Nat. Neurosci.* **13,** 133–140 (2010).
50. Bligh, E. G. & Dyer, W. J. A rapid method of total lipid extraction and purification. *Can. J. Biochem. Physiol.* **37,** 911–917 (1959).
51. Mason, R. J., Nellenbogen, J. & Clements, J. A. Isolation of disaturated phosphatidylcholine with osmium tetroxide. *J. Lipid Res.* **17,** 281–284 (1976).
52. Su, X. *et al.* Activation of the α7 nAChR reduces acid-induced acute lung injury in mice and rats. *Am. J. Respir. Cell Mol. Biol.* **37,** 186–192 (2007).
53. Langmead, B., Trapnell, C., Pop, M. & Salzberg, S. L. Ultrafast and memory-efficient alignment of short DNA sequences to the human genome. *Genome Biol.* **10,** R25 (2009).
54. Trapnell, C. *et al.* Transcript assembly and quantification by RNA-Seq reveals unannotated transcripts and isoform switching during cell differentiation. *Nat. Biotechnol.* **28,** 511–515 (2010).

nature cell biology

DOI: 10.1038/ncb3580

In the format provided by the authors and unedited.

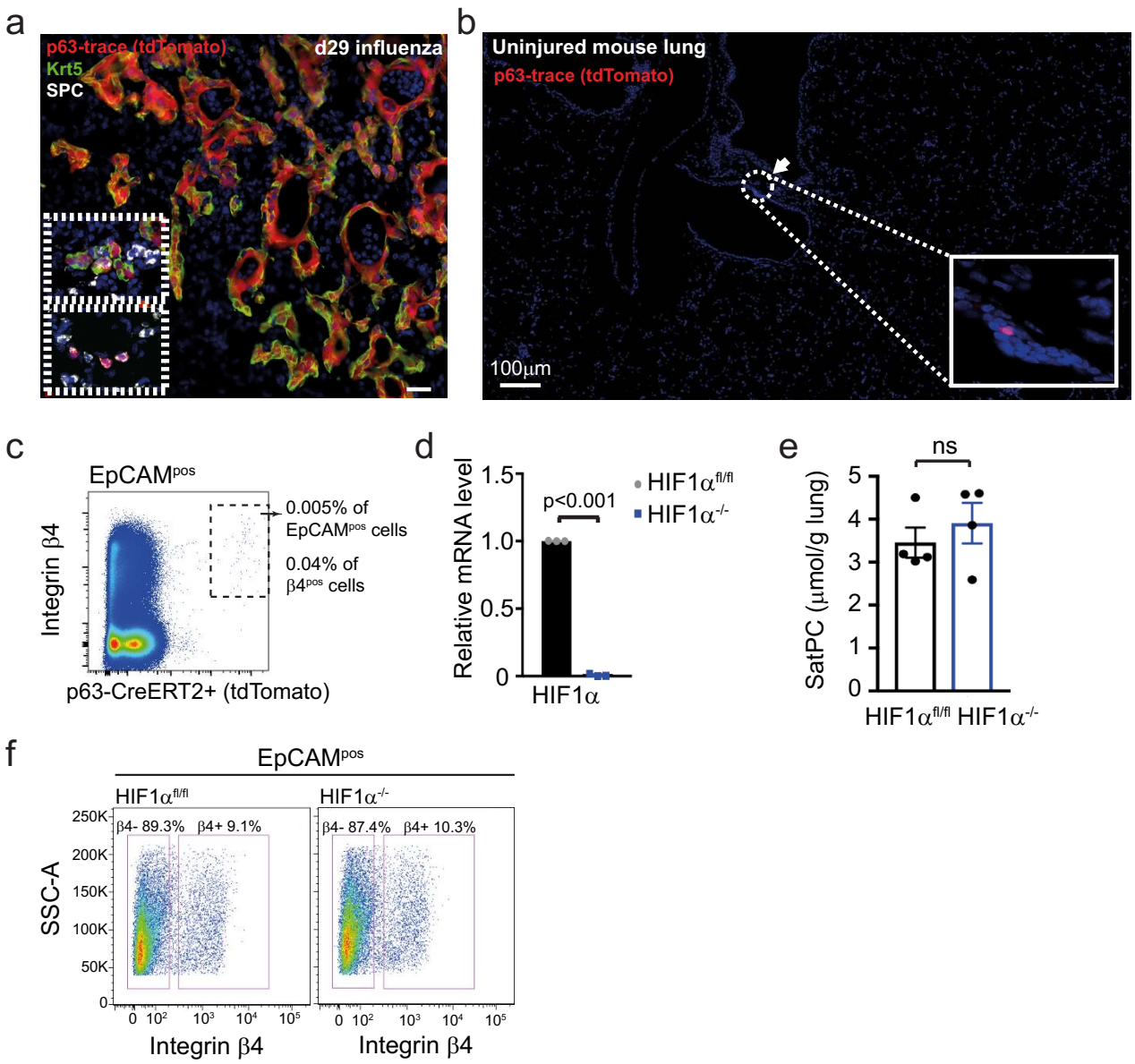

Supplementary Figure 1 p63^{pos} LNEPs are very rare and do not efficiently generate AEC2s. Lung epithelial ablation of HIF1α with Shh-Cre causes no defects in uninjured mice. (a) While p63^{pos} LNEPs generate Krt5 metaplasia, they make only a minor contribution to AEC2 regeneration after influenza injury (insets). (b) Rare p63-CreERT2 traced (tdTomato+) cells are scattered throughout airways in uninjured mice, representing 0.005% of the total epithelium as judged by FACS analysis (c). Data represent n=3 mice for histology (b), n=2 independent experiments with pooled live cells from 3 mice for FACS (c). (d) HIF1α is deleted in all the epithelial cells sorted from Shh-Cre; HIF1α$^{fl/fl}$ mouse lungs. Data are mean ± SEM from n=3 independent experiments, in which each group is a pool of 3 mice. (e) Lung SatPC content and (f) LNEP-enriched population (integrin β4^{pos} EpCAM^{pos}) remain unchanged after HIF1α deletion in epithelial cells. (e) Data are represented as mean ± SEM from n=4 mice per group from two independent experiments. (f) Data are represented as a percentage in EpCAM^{pos} live cells from a pool of 3 mice in each group. p values derived by unpaired two-tailed Student's t test.

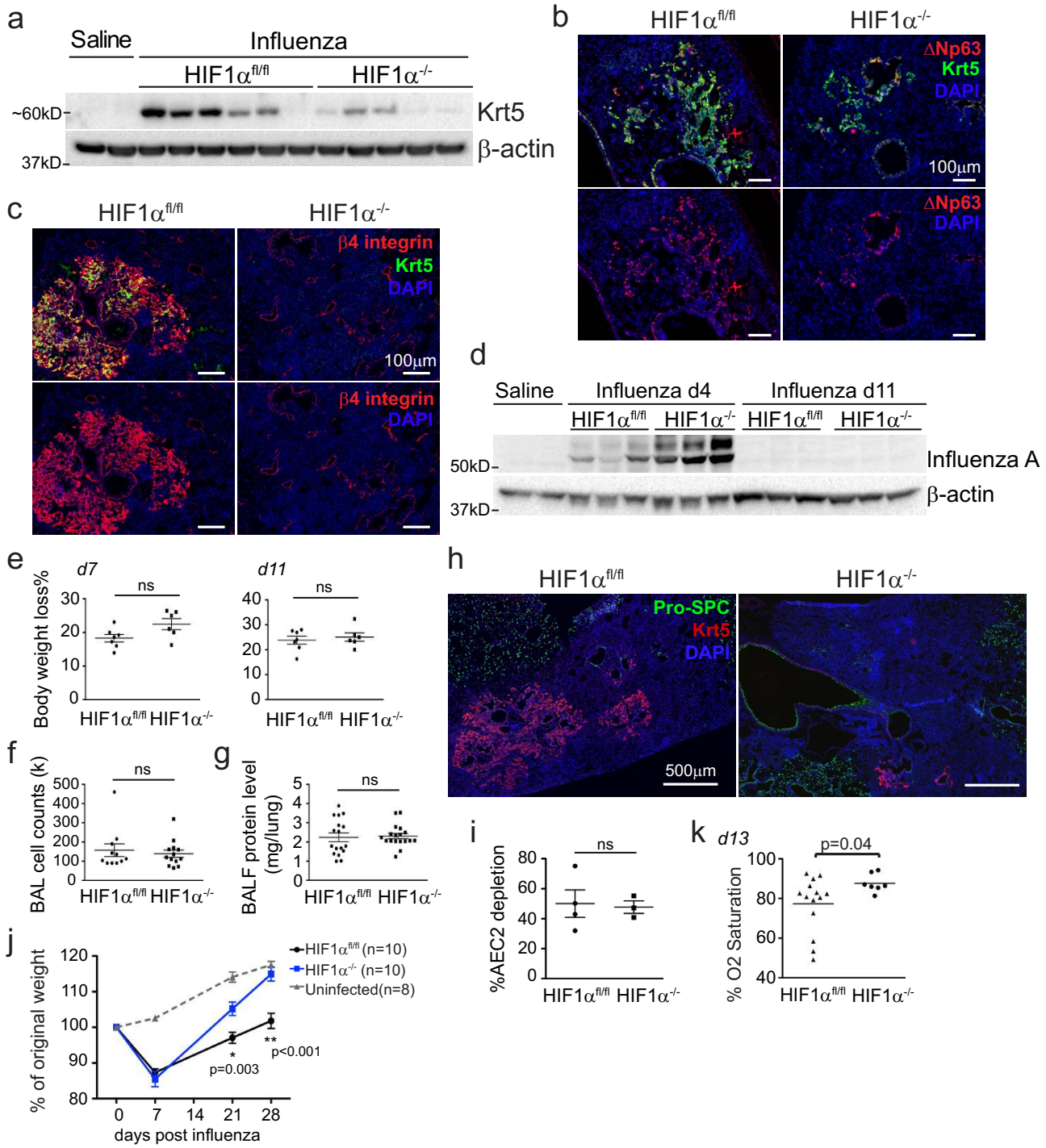

Supplementary Figure 2 HIF1α$^{-/-}$ mice are injured at similar levels as wild-type mice, but lack alveolar Krt5^{pos} cell expansion. (a) Representative blot showing Krt5 induction is inhibited by epithelial HIF1α deletion. (b-c) No large expansion of DNp63 (b) or integrin b4 (c) positive cells in the alveoli of HIF1α$^{-/-}$ mice, indicating alveolar Krt5^{pos} cell expansion is inhibited by HIF1α deletion. No difference in virus infection (d), weight loss (e), immune cell numbers in BAL (f) and BALF protein level (g) between wild-type and HIF1α$^{-/-}$ mice. (e-g) Data are represented as mean ± SEM, (e) n=7 wild-type, n=6 HIF1α$^{-/-}$; (f) n=11 wild-type, n=13 HIF1α$^{-/-}$; (g) n=17 wild-type, n=18 HIF1α$^{-/-}$ mice from three independent experiments. Each data point represents one mouse. (h) Large areas of AEC2 depletion are present in both wild-type and HIF1α$^{-/-}$ lungs, quantified in (i). SPC staining in airways (h, right) is an artifact of the goat anti-pro-SPC antibody. (i) Data are represented as mean ± SEM, n=4 wild-type, n=3 HIF1α$^{-/-}$ mice from 2 independent experiments. (j) HIF1α$^{-/-}$ mice recover weight more rapidly than their wild-type counterparts after influenza injury. Data are represented as mean ± SEM, n=10 wild-type, n=10 HIF1α$^{-/-}$, n=8 uninfected wild-type mice from three independent experiments. (k) Significant difference in average arterial oxygen saturation at 13 days post-infection between HIF1α$^{-/-}$ and wild-type mice. Each data point represents the average % O2 saturation reading for a single mouse at this time point (see Fig. 1h). Data are mean ± SEM, n= 7 HIF1α$^{-/-}$, n = 14 wild-type (2 Shh-Cre^{neg}, 12 C57BL6) mice from two independent experiments. Analysis is 11 days post-infection unless otherwise indicated. p values derived by unpaired two-tailed Student's t test, except in (k) derived by Mann Whitney.

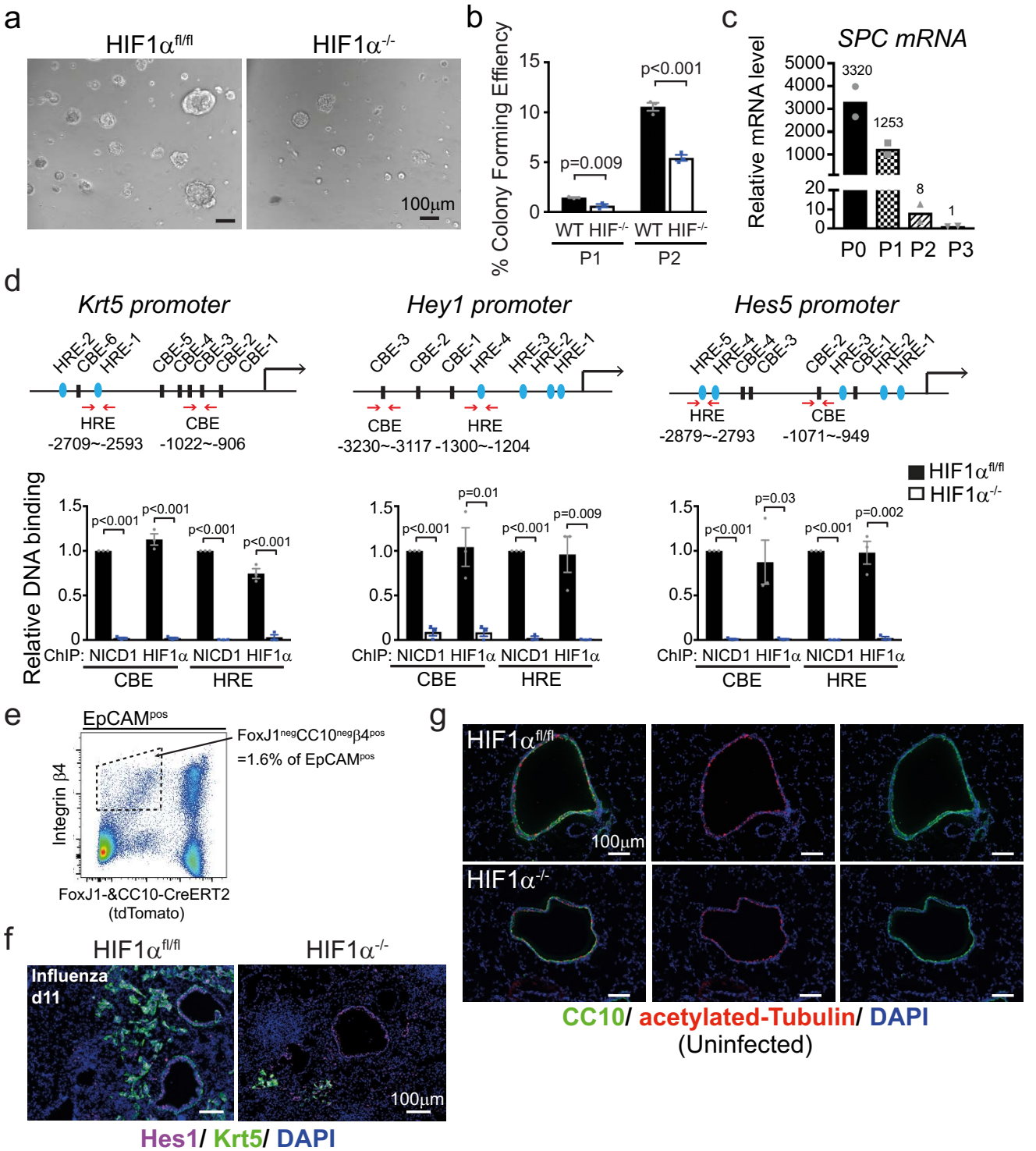

Supplementary Figure 3 HIF1α promotes Notch activity in LNEPs but has no effect on airway Notch activity. (a-b) Reduced colony size and number of HIF1α$^{-/-}$ LNEPs in culture. WT, HIF1α$^{fl/fl}$. (c) qPCR analysis of SPC in freshly sorted (P0) and cultured (P1-P3) LNEPs showing SPC mRNA dramatically decreases upon culture, n=2 independent experiments. (d) Top, mouse Krt5, Hey1 and Hes5 promoters contain HRE and CBE. The primers used in bottom are highlighted in red. Bottom, qPCR analysis of ChIP demonstrating HIF1α deletion blocks NICD1 DNA binding on Krt5, Hey1 and Hes5 promoters in cultured LNEPs. Ct value of pulled down DNA was normalized by Ct of input DNA and the abundance was calculated relative to NICD1 association of each site. (b,d) Data are represented as mean ± SEM from n=3 independent experiments. p values derived by unpaired two-tailed Student's t test. (e) FACS isolation of highly purified LNEPS (FoxJ1^{neg} CC10^{neg} integrin β4+) from uninjured mice used for RNA-Seq analysis. (f) HIF1α deletion inhibits Hes1 staining in the alveoli but not airways. (g) HIF1α deletion has no effect on airway Notch activity in uninfected mice, as judged by the ratio between club cells (CC10^{pos}) and multi-ciliated cells (acetylated-Tubulin^{pos}) remaining unchanged.

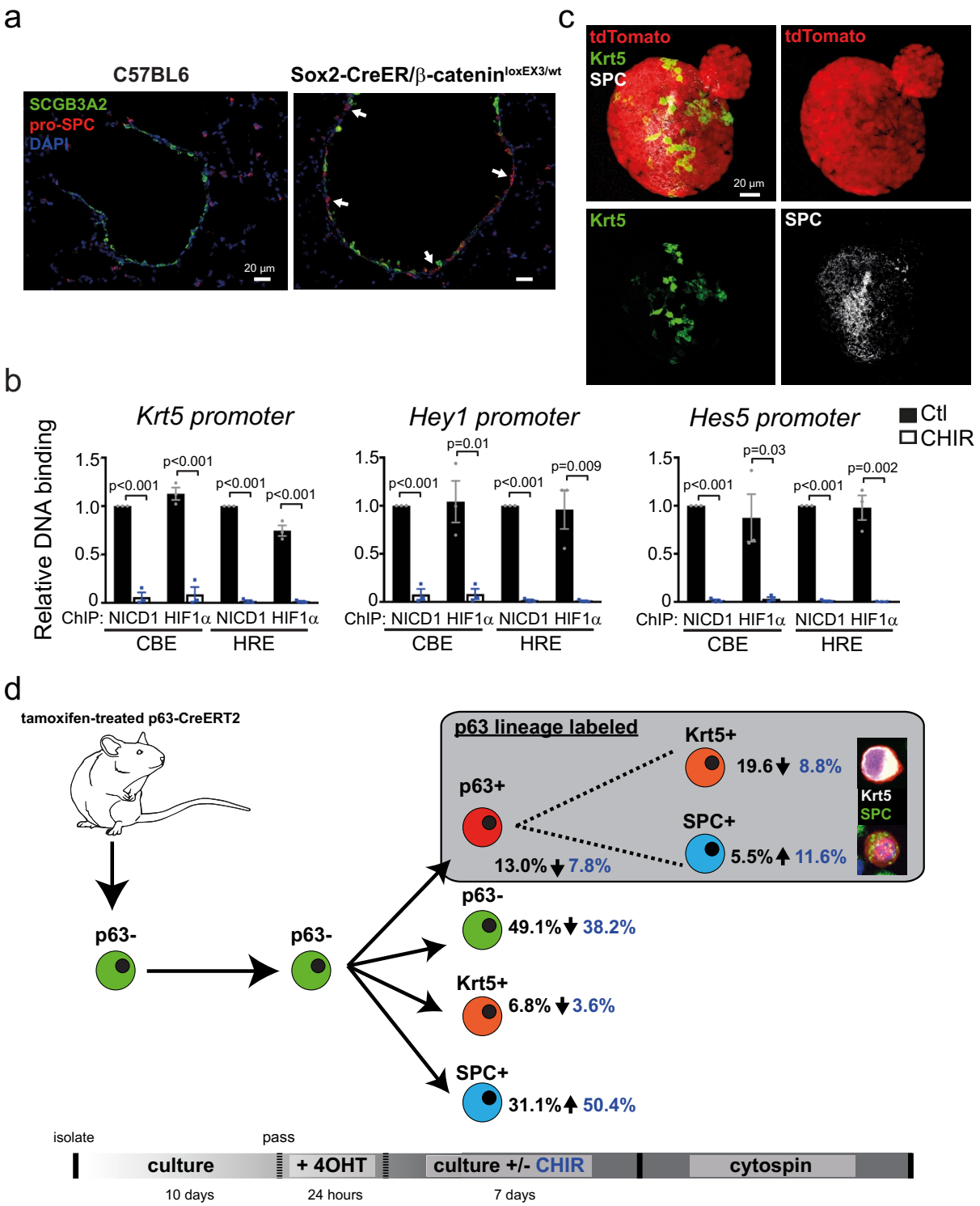

Supplementary Figure 4 Stabilization of b-catenin inhibits Notch and HIF1α activity by blocking their DNA association. (a) β-catenin stabilization increases ectopic SPC expression in the airways largely independent of club cells expressing Scgb3a2. About 27% (97 cells out of 362) Sox2-traced airway cells express SPC 7 days after tamoxifen induced β-catenin stabilization, n = 3 mice examined. (b) qPCR analysis of ChIP demonstrating NICD1 and HIF1a DNA binding on Krt5, Hey1 and Hes5 promoters are blocked by CHIR. The same control sample (LNEPs from HIF1α$^{fl/fl}$ mice) was used as Supplementary Fig. 3d. Data are represented as mean ± SEM from n=3 independent experiments. p values derived by unpaired two-tailed Student's t test. (c) Individual fluorescent channels of the colony from Fig. 3g demonstrating Krt5 and SPC expression in a single clone. (d) p63^{neg} LNEPs *in vitro* either remain undifferentiated, are activated into p63^{pos} cells (visualized by tdTomato expression after a brief 4OHT treatment), or differentiate into Krt5+ or SPC+ cells. Wnt agonism (blue) results in more SPC+ cells and fewer Krt5+ cells as described in Fig. 4d. Grey inset quantifies these outcomes specifically within those cells that become p63 traced. Quantification is via immunostaining of cytospins, n=2 experiments.

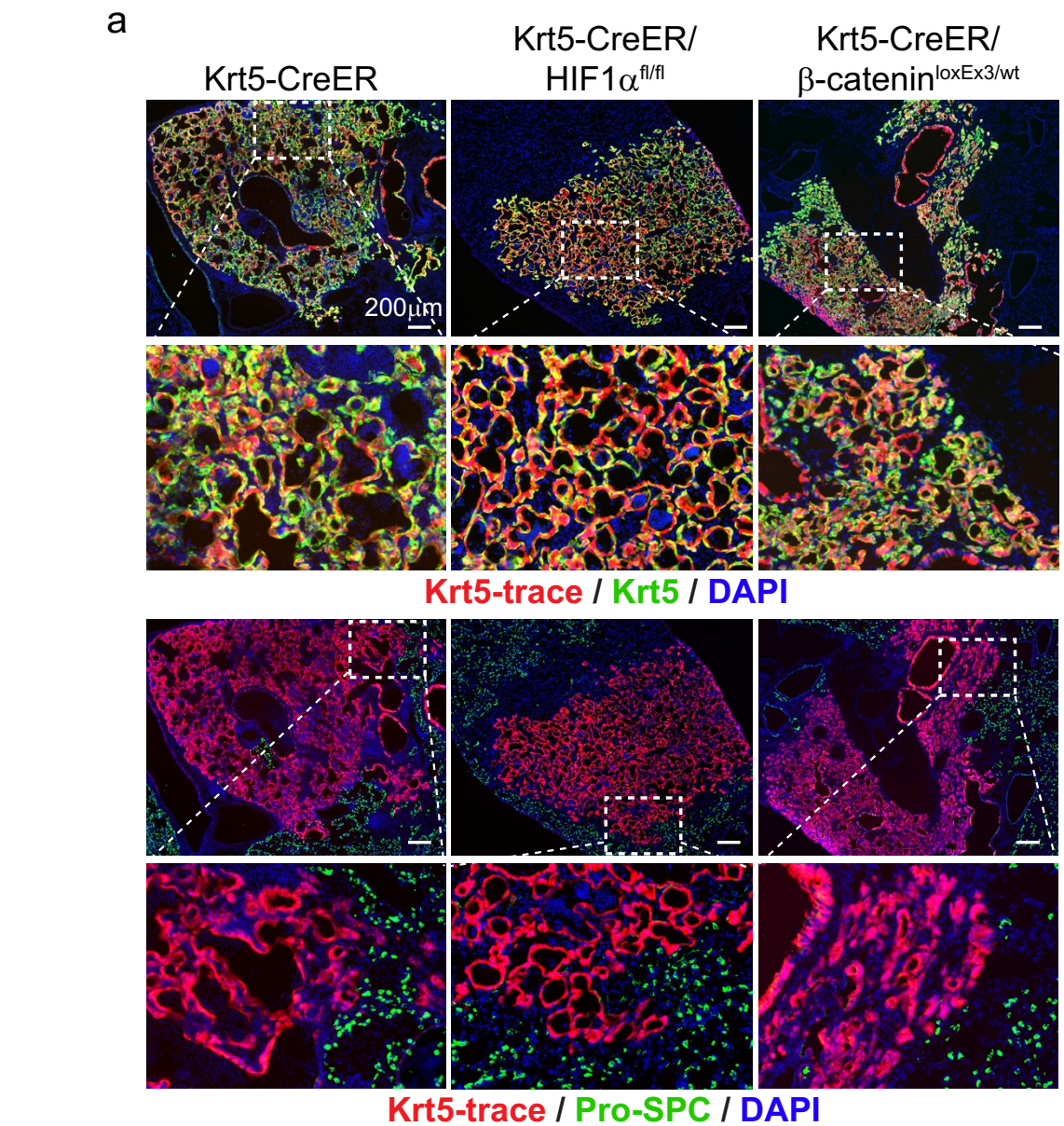

b

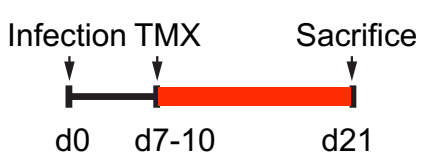

c Relative mRNA level

	Krt5-trace	Krt5-trace; HIF1α fl/fl
Hey1	1.0	1.9
Hey2	1.0	1.2
Hes5	1.0	4.0
HIF1α	1.0	0.1

d Relative mRNA level

	Krt5-trace	Krt5-trace; loxEx3
Hey1	1.0	0.9
Hey2	1.0	0.4
Hes5	1.0	0.9
Axin2	1.0	32280.3

Supplementary Figure 5 Deleting HIF1α or stabilizing b-catenin does not alter LNEP differentiation after full Notch/Krt5 activation. (a) HIF1a deletion or β-catenin stabilization subsequent to Krt5 activation as described in (b) has no effect on Krt5 (green, upper panel) and SPC (green, lower panel) expression. (c) Relative mRNA levels in sorted Krt5-CreERT2-traced cells 21 days post infection with (n=8) or without (n=2) HIF1α deletion. Notch activity is not downregulated by HIF1α deletion in Krt5 expressing cells. (d) Relative mRNA levels in sorted Krt5 traced cells 21 days post infection with (n=2) or without (n=5) b-catenin stabilization. Notch activity is not inhibited by Wnt signaling in Krt5 expressing cells. (c-d) Sorted cells from two independent experiments were pooled together for RNA isolation.

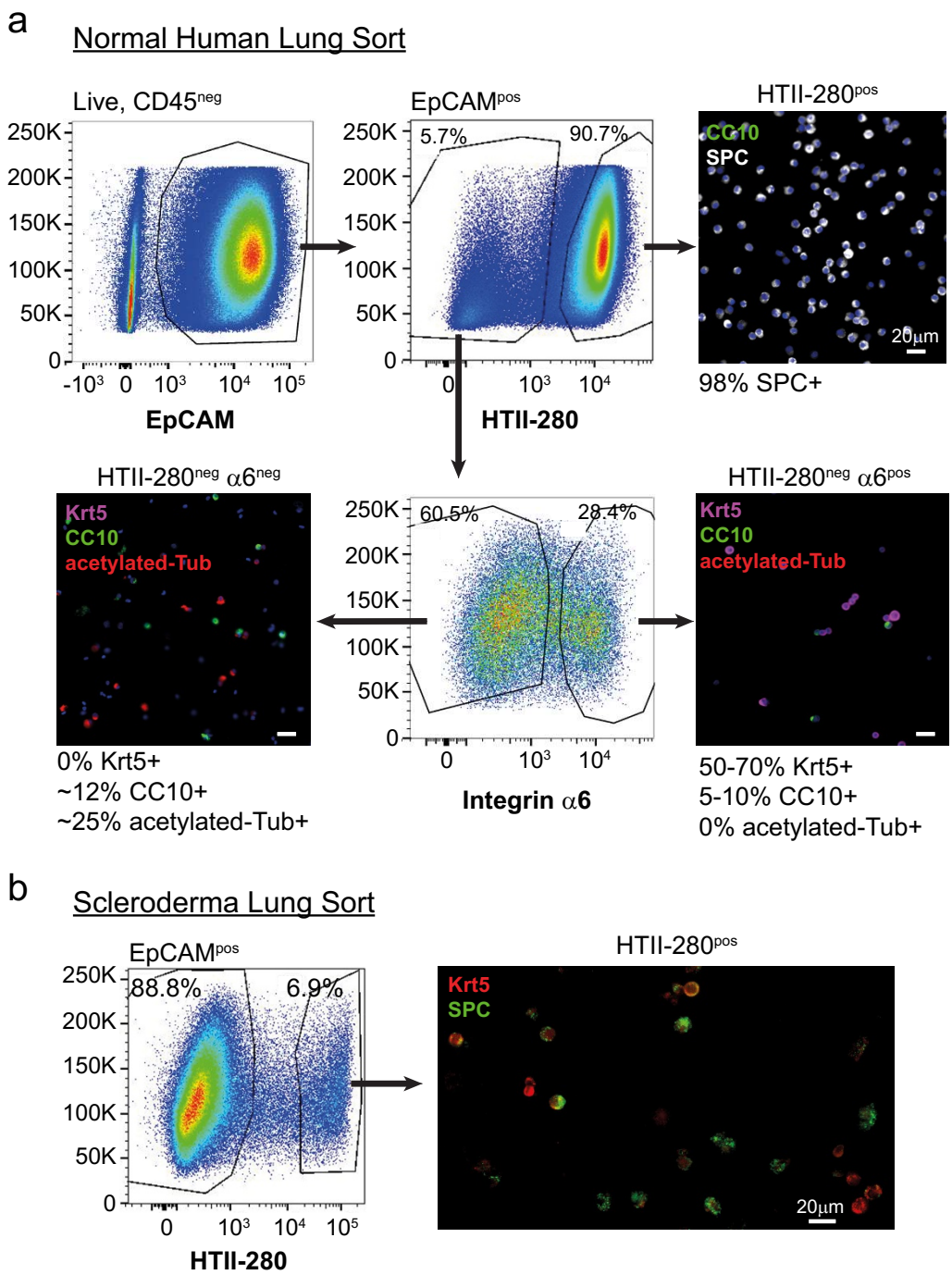

Supplementary Figure 6 Flow plots and cytospin of human lung epithelial cell sort. (a) As judged by cytospin, the HTII-280^{pos} population captures all the SPC^{pos} AEC2s, and the HTII-280$^{neg}\alpha6^{pos}$ population is enriched for basal cells in normal human lungs. (b) In scleroderma lung, the percentage of HTII-280^{pos} cells as a function of total EpCAM^{pos} cells decreases and both Krt5^{pos} and Krt5/SPC double positive cells are observed in HTII-280^{pos} cells.

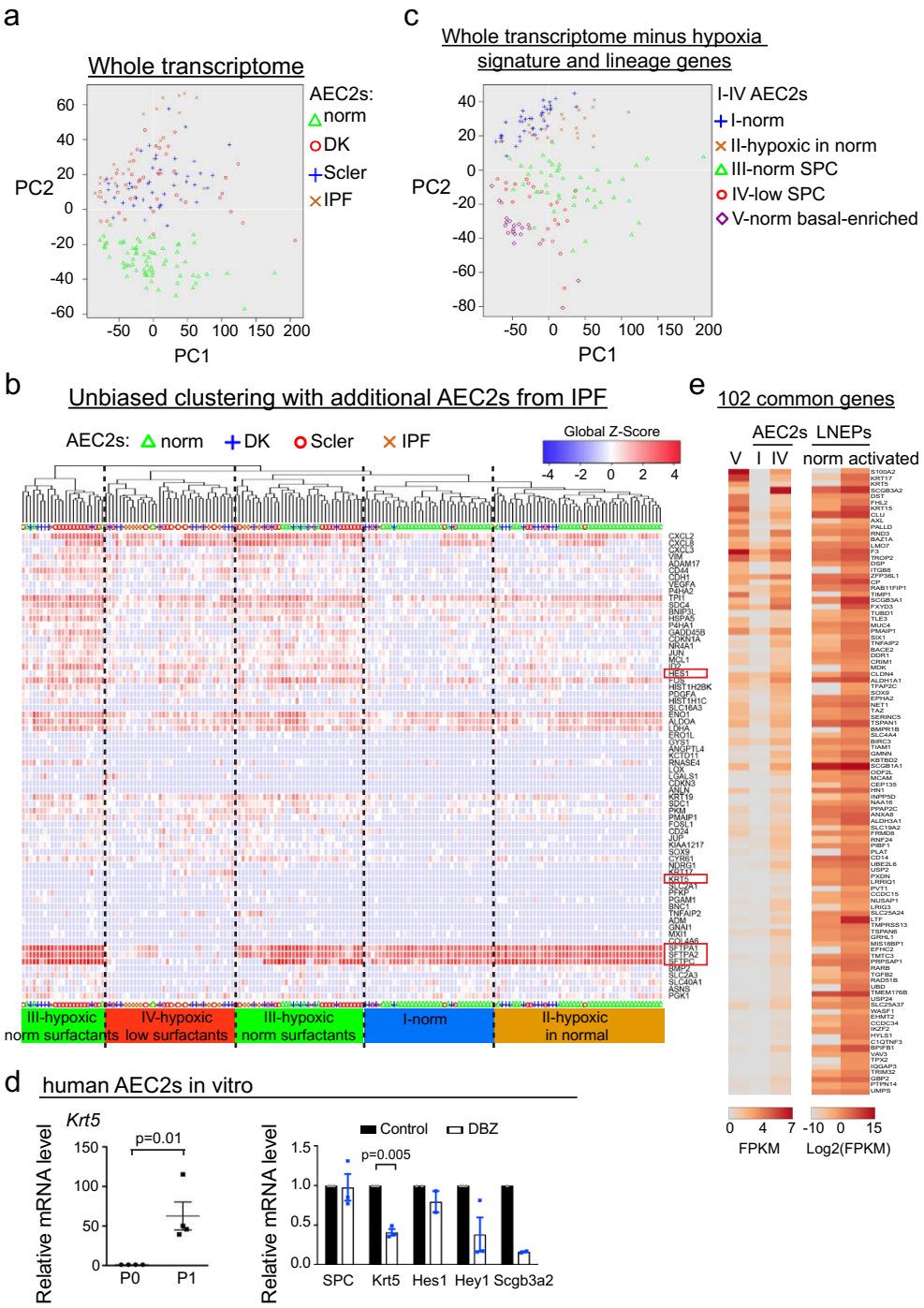

Supplementary Figure 7 Transdifferentiation of human AEC2s to basal-like cells and single cell RNA-Seq analysis of primary human lung epithelial cells show distinct hypoxia signature in fibrotic lungs. (a) Whole-genome wide PCA analysis of HTII-280^{pos} cells from normal, DK, Scleroderma and IPF lungs, showing AEC2s from fibrotic lungs are distinct from that of normal lungs. (b) Hierarchical clustering of single cell transcriptomes of HTII-280^{pos} cells isolated from normal, DK, scleroderma and IPF lungs. Listed genes (rows) are hypoxia signature (listed in Figure 5c) plus *STFPA1, STFPA2, SFTPC, KRT5, HES1* (highlighted with red rectangles). Four distinct groups (I-IV) are highlighted. Cells from IPF lungs are mostly in Group IV. (c) PCA analysis of all human cells using the entire genome except for the signature genes from Fig. 6a, demonstrating that the hypoxia & lineage gene set is predictive of meaningful differences in cell identity at the whole-transcriptome level. (d) Primary human AEC2s (HTII-280^{pos}) upregulated Krt5 mRNA after one passage in culture by qPCR analysis. Notch inhibition (DBZ) during this initial culture attenuated Krt5 upregulation (right). Data are represented as mean ± SEM, where each point represents one independent cell isolation and experiment (n=4 left, n=3 right). p values derived by unpaired two-tailed Student's t test (d, left) or one-sample t-test (d, right). (e) Average FPKM values of human cells (Group I, IV and V), and mouse quiescent and activated LNEPs from RNA-seq are indicated in the heatmap (right) for the shared upregulated 102 gene set (see Fig. 7).

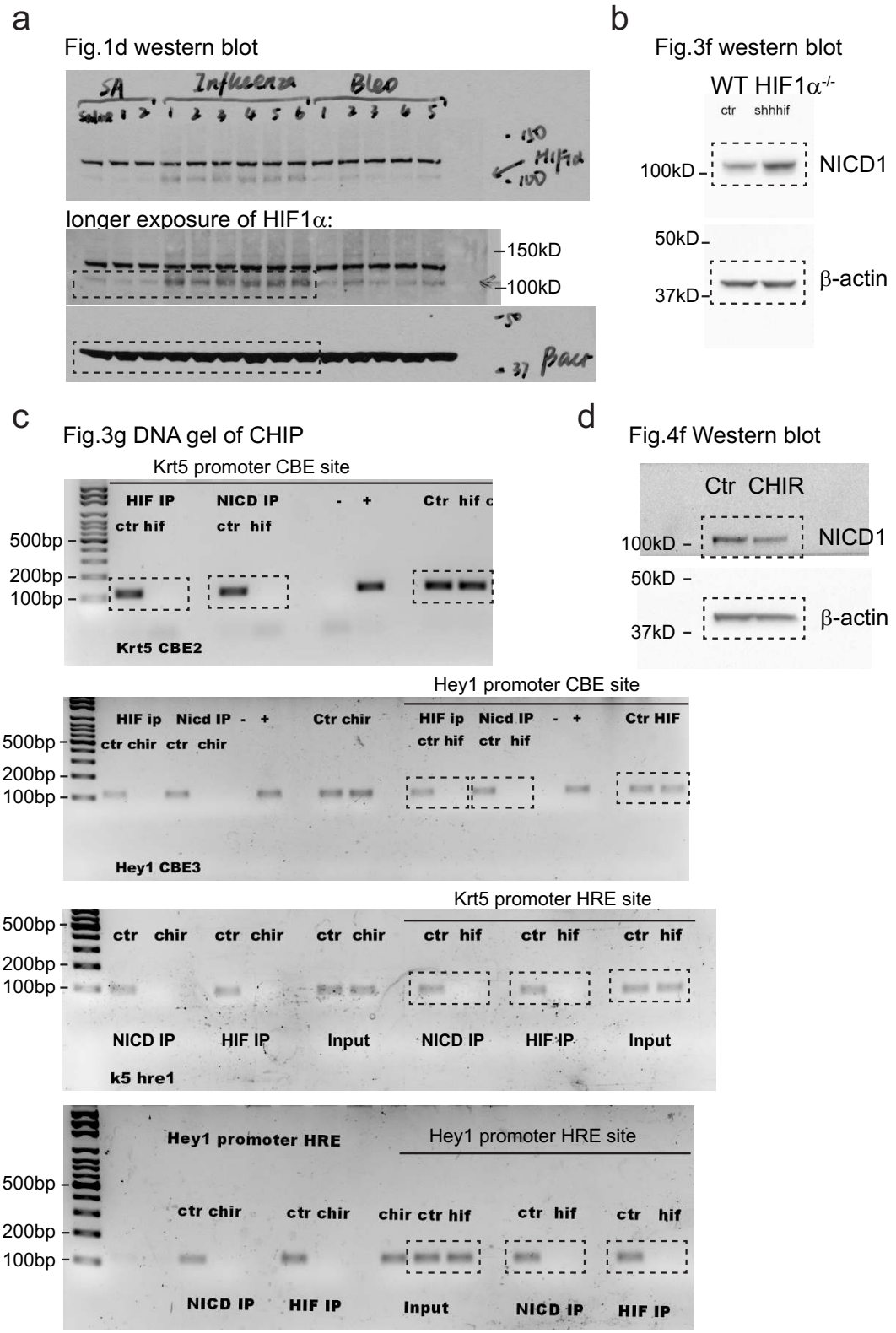

Supplementary Figure 8 Unprocessed original scans of immunoblots and agarose gel electrophoresis images. (a,b,d,f,g,h) Unprocessed western blot scans for Figures 1d, 3f, 4f, 5d, S2a and S2d. (c, e) Unprocessed DNA gel electrophoresis of ChIP for Figures 3g and 4e.

e

Fig.4e DNA gel of CHIP

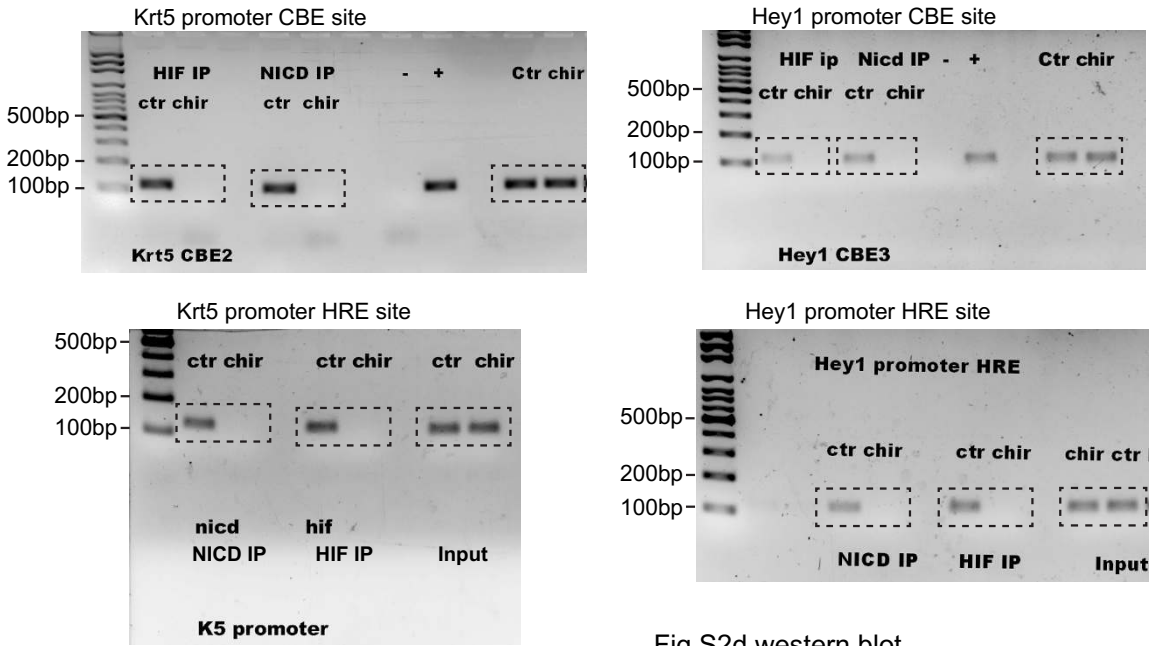

f

Fig.5d Western blot

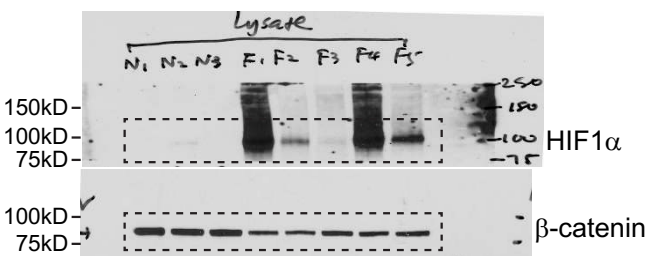

g

Fig.S2a western blot

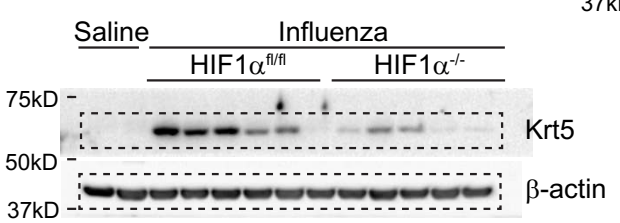

h

Fig.S2d western blot

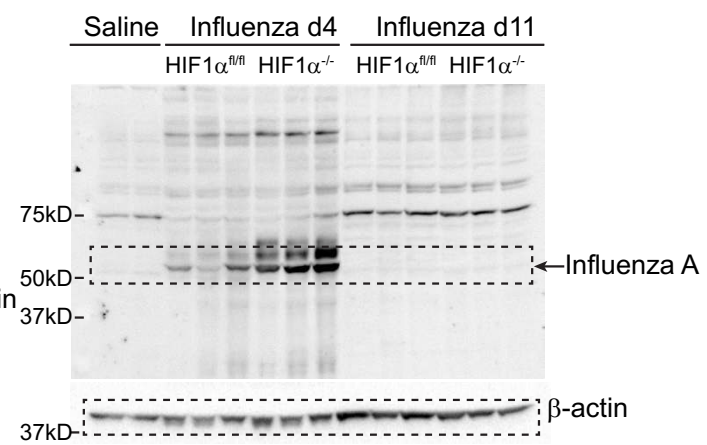

Supplementary Figure 8 Continued

SUPPLEMENTARY INFORMATION

Supplementary Tables Legends

Supplementary Table 1 Top 100 differentially expressed genes between normal and diseased human AEC2s (HTII-280^{pos}).

Supplementary Table 2 Top upstream regulators of human diseased versus normal AEC2s (HTII-280^{pos}) from IPA® analysis.

Supplementary Table 3 Expression of hypoxia signature plus *HES1*, makers of basal cells and AEC2s in normal and diseased human AEC2s (HTII-280^{pos}).

Supplementary Table 4 Top 100 differentially expressed genes in Group I-V cells.

Supplementary Table 5 Expression of top differentially expressed genes and motility genes in Group I, III, IV and V cells.

Supplementary Table 6 Upregulated and downregulated genes shared by activated LNEPs and Group IV hypoxic AEC2s.

Supplementary Table 7 Top upstream regulators of the 102 common genes from IPA® analysis (see excel).

Supplementary Table 8 Pathway analysis of the 102 common genes from IPA® analysis (see excel).

Supplementary Table 9 Diseases and functions affected by the 102 common genes from IPA® analysis (see excel).

Supplementary Table 10 Primers.

Supplementary Table 11 Statistics Source Data.

nature research

Corresponding Author: Harold A. Chapman

Date: Jun 5, 2017

Life Sciences Reporting Summary

Nature Research wishes to improve the reproducibility of the work we publish. This form is published with all life science papers and is intended to promote consistency and transparency in reporting. All life sciences submissions use this form; while some list items might not apply to an individual manuscript, all fields must be completed for clarity.

For further information on the points included in this form, see Reporting Life Sciences Research. For further information on Nature Research policies, including our data availability policy, see Authors & Referees and the Editorial Policy Checklist.

Experimental design

1. Sample size

   Describe how sample size was determined.

   No statistical method was used to predetermine sample size. The sample size was determined on the basis of our prior knowledge of the variability of experimental output and on initial results or pilot experiments for each line of in vitro or in vivo experiments reported.

2. Data exclusions

   Describe any data exclusions.

   No data were excluded from analyses.

3. Replication

   Describe whether the experimental findings were reliably reproduced.

   All attempts at replication were successful.

4. Randomization

   Describe how samples/organisms/participants were allocated into experimental groups.

   The experiment were not randomized.

5. Blinding

   Describe whether the investigators were blinded to group allocation during data collection and/or analysis.

   The investigators were not blinded to group allocation during data collection and/or analysis.

   Note: all studies involving animals and/or human research participants must disclose whether blinding and randomization were used.

6. Statistical parameters

   For all figures and tables that use statistical methods, confirm that the following items are present in relevant figure legends (or the Methods section if additional space is needed).

n/a	Confirmed	
☐	☒	The exact sample size (*n*) for each experimental group/condition, given as a discrete number and unit of measurement (animals, litters, cultures, etc.)
☐	☒	A description of how samples were collected, noting whether measurements were taken from distinct samples or whether the same sample was measured repeatedly.
☐	☒	A statement indicating how many times each experiment was replicated
☐	☒	The statistical test(s) used and whether they are one- or two-sided (note: only common tests should be described solely by name; more complex techniques should be described in the Methods section)
☐	☒	A description of any assumptions or corrections, such as an adjustment for multiple comparisons
☐	☒	The test results (e.g. *p* values) given as exact values whenever possible and with confidence intervals noted
☐	☒	A summary of the descriptive statistics, including central tendency (e.g. median, mean) and variation (e.g. standard deviation, interquartile range)
☐	☒	Clearly defined error bars

See the web collection on statistics for biologists for further resources and guidance.

Software

Policy information about availability of computer code

7. Software

Describe the software used to analyze the data in this study.	Only commercially available or free software was used for data analysis. This includes Graphpad Prism, Fluidigm Singular, FlowJo, and Microsoft Excel.

For all studies, we encourage code deposition in a community repository (e.g. GitHub). Authors must make computer code available to editors and reviewers upon request. The *Nature Methods* guidance for providing algorithms and software for publication may be useful for any submission.

Materials and reagents

Policy information about availability of materials

8. Materials availability

Indicate whether there are restrictions on availability of unique materials or if these materials are only available for distribution by a for-profit company.	Goat anti-CC10 antibody was a gift from Dr. Barry Stripp and HTII-280 antibody was a gift from Dr. Leland Dobbs.

9. Antibodies

Describe the antibodies used and how they were validated for use in the system under study (i.e. assay and species).	IF: rabbit anti-pro-SPC (1:3000; Millipore, #AB3786), goat anti-pro-SPC (1:2000; Santa Cruz, #SC-7706), rabbit anti-Krt5 (1:1000; Covance, #PRB-160P), chicken anti-Krt5 (1:1000; Covance, #SIG-3475), rabbit anti-ΔNp63 (1:100; Cell Signaling, #13109), rat anti-mouse integrin β4 (1:200; BD, #555721), goat anti-CC10 (1:10,000, a gift from Dr. B. Stripp), mouse anti-acetylated tubulin (1:500, Sigma, 6-11B-1), rat anti-E-cadherin (1:500, Invitrogen, #13-1900), rabbit anti-Hes1 (1:1000; Cell Signaling, #11988), goat anti-Scgb3a2 (1:100, R&D, AF3465). Western blots: HIF1α (1:500, R&D systems, #AF1935), pro-SPC (1:500, Millipore, #AB3786), Krt5 (1:1000, Covance, #PRB-160P), Cleaved Notch1 (1:1000, Cell signaling, #4147), E-cadherin (1:2000, BD, #610181), ?-actin (1:10000, Sigma-Aldrich, #A5441). To detect influenza A virus, unboiled lysates in 1mM DTT and 2% SDS were blotted with anti-Influenza A antibody (1:1000, Millipore, #AB1074). FACS: rat anti-mouse CD45 (1:200, BD, #553078), rat anti-mouse CD16/CD32 (1:200, BD, #553143), rat anti-mouse CD31 (1:200, BD, #553371), then incubated for 1 hr at 4°C with the following primary antibodies or viability dye diluted in DMEM (without phenol red) plus 2% FBS (Gibco): phycoerythrin (PE) or BV421-conjugated rat anti-mouse EpCAM (1:500; Biolegend, #563477, #563214), Alexa Fluor® 647 or PE-conjugated rat anti-mouse integrin β4 (1:75; BD, #553745), fixable viability dye eFluor® 780 (1:2000, eBioscience), Goat anti-pro-SPC (1:500; Santa Cruz, #SC-7706), BV421 rat anti-mouse EpCAM, Alexa Fluor® 488 donkey anti-goat IgG (1:2000, ThermoFisher, #A-11055). Validation for species and application was from manufacturer website.

10. Eukaryotic cell lines

a. State the source of each eukaryotic cell line used.	No eukaryotic cell line was used.
b. Describe the method of cell line authentication used.	No eukaryotic cell line was used.
c. Report whether the cell lines were tested for mycoplasma contamination.	No eukaryotic cell line was used.
d. If any of the cell lines used in the paper are listed in the database of commonly misidentified cell lines maintained by ICLAC, provide a scientific rationale for their use.	No commonly misidentified cell lines were used.

Animals and human research participants

Policy information about studies involving animals; when reporting animal research, follow the ARRIVE guidelines

11. Description of research animals

Provide details on animals and/or animal-derived materials used in the study.

HIF1αfl/fl, Shh-Cre, Krt5-CreERT2, Sox2-CreERT2, β-cateninloxEx3, CC10-CreERT, FoxJ1-CreERT2, p63-CreERT2, Ub-GFP, SPC-CreERT2, and Ai14-tdTomato mice were used in the study and they were all previously described. For all experiments, 6–8 week old animals of both sexes were used in equal proportions.

Policy information about studies involving human research participants

12. Description of human research participants

Describe the covariate-relevant population characteristics of the human research participants.

The study did not involved human research participants. All human samples are non-identified, otherwise discarded tissues.

nature research

Corresponding Author: Hal Chapman

Date: Jun 6, 2017

Flow Cytometry Reporting Summary

Form fields will expand as needed. Please do not leave fields blank.

Data presentation

For all flow cytometry data, confirm that:

☒ 1. The axis labels state the marker and fluorochrome used (e.g. CD4-FITC).

☒ 2. The axis scales are clearly visible. Include numbers along axes only for bottom left plot of group (a 'group' is an analysis of identical markers).

☒ 3. All plots are contour plots with outliers or pseudocolor plots.

☒ 4. A numerical value for number of cells or percentage (with statistics) is provided.

Methodological details

5. Describe the sample preparation.	Lung epithelial cells were obtained by Dispase digestion of primary tissue, exactly as described in Methods.
6. Identify the instrument used for data collection.	All data was collected on either FACSAria II or LSR II.
7. Describe the software used to collect and analyze the flow cytometry data.	Analysis was performed using FlowJo.
8. Describe the abundance of the relevant cell populations within post-sort fractions.	Purity checks were routinely performed by re-running ~100-500 sorted cells back through the sorter and ensuring they fell within appropriate gates.
9. Describe the gating strategy used.	As a general rule cells were gated on forward and side scatter corresponding to the known scatter profile of lung epithelial cells. Next they were gated as singlets, and then gated as live (viability dye negative) and CD45 negative. All positive gates were based off of the background fluorescence signal obtained by staining with an isotype antibody conjugated to the same fluorophore as the primary antibody.

Tick this box to confirm that a figure exemplifying the gating strategy is provided in the Supplementary Information. ☒